Ph.D. Dissertation of Engineering

Evaluation of soil organic carbon stocks in heterogeneous land cover types towards carbon neutral city

탄소 중립 도시를 위한 이질적 도시 피복 내 토양 유기 탄소 저장량 평가

August 2021

Graduate School of Seoul National University
Interdisciplinary Program in
Landscape Architecture

Jeehwan Bae

Evaluation of soil organic carbon stocks in heterogeneous land cover types towards carbon neutral city

Advisor: Youngryel Ryu

A dissertation submitted in partial fulfillment of the requirements for the Degree of Doctor of Philosophy in Interdisciplinary Program in Landscape Architecture in Seoul National University

August 2021

Jeehwan Bae

Approved by Thesis Committee

Chair _____

Vice Chair _____

Examiner _____

Examiner _____

Examiner _____

Abstract

Evaluation of soil organic carbon stocks in heterogeneous land cover types towards carbon neutral city

Jeehwan Bae
Interdisciplinary Program in Landscape Architecture in
Seoul National University
Graduate School of Seoul National University
Supervised by Professor Youngryel Ryu

Soils hold the largest organic carbon in urban ecosystem. Quantifying urban soil organic carbon (SOC) stocks is a preliminary step for carbon neutral strategy in urban ecosystem. The impacts of urbanization on SOC stocks have gained attention from policy makers as well as land managers. However, urban SOC stocks are often omitted from estimates of carbon budgets in urban area due to the small sample size and high degree of variability under heterogeneous land–cover types.

In this dissertation, I aimed to find the spatial and vertical variations of urban SOC stocks. Understanding how SOC stocks in heterogeneous land–cover types is essential to assess urban carbon storage; however, the spatial and vertical distributions of SOC stocks have been poorly characterized. Intensive urbanization, and underground development in particular, leads to spatial and vertical heterogeneity of SOC. The magnitude and origin of SOC under different urban setting have not been well explored.

In Chapter 2, I quantified SOC stocks to a 5 m depth beneath impervious surfaces and adjacent vegetative surfaces at three housing complexes in Seoul Special City, Republic of Korea. The objectives of Chapter 2 were (1) to quantify the spatial and vertical distribution of SOC stocks beneath impervious surfaces and

vegetative surfaces; (2) to investigate the key factors that control the spatial and vertical distribution of SOC stocks; and (3) to understand how anthropogenic factors affect SOC stocks in heterogeneous urban setting. In the top 1 m of the profile, SOC stocks under vegetative surfaces were three times greater than those under impervious surfaces. However, we discovered that unexpectedly high SOC stocks appeared in deeper soil layers under both surface types, which led to comparable SOC stocks at a depth of 5 m beneath the impervious surface (16.9 ± 1.9 kgC m^{-2}) and at the vegetative surface (22.3 ± 2.2 kgC m^{-2}). Consequently, the ratio of SOC stocks at depths of 1 m to 5 m were 16% in impervious surfaces and 34% in vegetative surfaces, suggesting conventional soil sampling at 1 m depth could miss large SOC. Stable isotope data ($\delta^{13}C$ and $\delta^{15}N$) combined with historical aerial photographs revealed that cropland that existed until the 1970s formed the high SOC cultural layer in deeper soils. Our results highlight that deep soils under impervious surfaces could be overlooked carbon hotspots in urban ecosystems. We believe this finding could help city planners and policy makers to assess regional carbon budgets and to reduce carbon footprint by recycling the deep SOC excavated from various construction projects towards sustainable urban development.

Landscape fragmentation has created large areas of forest edge. Understanding how SOC stocks within forest edges respond to fragmentation is essential to assess carbon budgets; however, the causes and magnitude of edge effects on SOC stocks have been poorly characterized. The goal of **Chapter 3** is to assess the edge effects on SOC stocks in fragmented urban–rural forests. Here, I quantified the edge effects on SOC stocks along an urban–rural gradient from three fragmented urban forests to a large patch of rural forest. The SOC stocks within 20 m of the rural forest edge (1.86 kgC m^{-2}) is on average 80% lower than the interiors of rural forest (10.47 kgC m^{-2}). We found that biotic factors, including annual litterfall mass ($R^2 > 0.94$), peak leaf area index ($R^2 > 0.92$), and fine-root mass density ($R^2 > 0.77$), explained the spatial variation in SOC

stocks within the rural forest. In urban forests, human activities at forest edges led to contrasting edge effects on SOC stocks, for instance, the SOC stocks at the east edges (4.74 kgC m^{-2}) were over 63% greater than at the west edges (2.9 kgC m^{-2}) explained by the adjacent land uses (e.g., paved roads vs. non-paved soils) and in-situ litterfall management. We also found significant differences in summer soil temperature (ΔT_S > 2.8℃) and soil moisture (ΔVWC > 0.05 m^3 m^{-3}) between the east and west forest edges. Our results reveal that the factors responsible for the edge effects on SOC stocks in rural forests are biotic factors, while heterogeneous human activities at the local scale lead to complex edge effects on urban forest SOC stocks.

Urban soil is a heterogeneous mixture of various parent materials and significantly affected by anthropogenic activities. Improving our understanding of the relationships between the pattern of land use and the SOC stocks requires large amounts of timely and cost efficient SOC analysis, which is difficult to obtain with routine chemical analysis. In Chapter 4, I evaluated a predictive model for SOC based on hyperspectral reflectance dataset in urban soils using ASD-FieldSpec, then used partial least squares (PLS) regression to establish the predictive models for SOC in urban soils. A total of 136 samples were collected and the SOC and $\delta^{13}C$ values of topsoil (0-20 cm) were measured under different land cover types. The SOC stocks varied between 0.33 kg m^{-2} to 12.51 kg m^{-2}. The $\delta^{13}C$ data varied between −30.18‰ to −17.17‰. The average SOC and $\delta^{13}C$ data showed a clear vegetation-dependent pattern. The PLSR model achieved acceptable results with coefficient of determination (R^2) and root mean square error (RMSE) of calibration set for SOC (R^2 = 0.83; RMSE = 1.6%). The leave one out cross validation procedure confirmed the robust performance of PLS model. The results indicated that 1) the SOC can be estimated with reasonable accuracy across heterogeneous urban land-cover types based solely on the hyperspectral reflectance spectroscopy, and 2) the strategy has the potential of upscaling for city scale assessments of SOC stocks.

Keyword: Urbanization, Land cover change, Urban soils, Soil organic carbon stocks, Urban deep soils, Edge effect, Stable isotope technology, Soil spectroscopy

Student Number : 2019-32756

Table of Contents

Abstract iii

Chapter 1. Introduction 2

1. Background 2
   1.1. Urbanization and the cultural layers of SOC stocks 2
   1.2. Edge effects on SOC stocks in fragmented urban landscpae 3
   1.3. Landscape-scale assessments of SOC via hyperspectral data 3
2. Purpose 4

Chapter 2. High soil organic carbon stocks under impervious surfaces contributed by urban deep cultural layers 8

1. Introduction 8
2. Methods and materials 9
   2.1 Site description 9
   2.2 Data collection 11
   2.3. Data processing 11
   2.4. Statistical analyses 12
3. Results 13
   3.1. Vertical dsitributions of soil bulk density, SOC concentration and fine roots 13
   3.2. Vertical distributions of SOC stocks 15
   3.3. Depth profiles of soil carbon and nitrogen isotopes 16
4. Discussion 17
   4.1 What controls vertical heterogeneity of urban SOC stocks? 17
   4.2 How does the impervious surfaces affect the urban SOC stocks? 20
   4.3 How can deep SOC data be used for sustainable urban development? 22
5. Conclusions 23

Chapter 3. The magnitude and causes of edge effects on soil organic carbon stocks along an urban-rural gradient 24

1. Introduction 24
2. Methods and Materials 27
   2.1. Site description 27
   2.2. Data collection 29
   2.3. Data processing 31
   2.4. Statistical analyses 32
3. Results 33

3.1. Soil organic carbon (SOC) stocks along an urban-rural gradient…33
3.2. The spatiotemporal variation of abiotic factors across urban and rural forests 34
3.3. Relationships between spatial variation of biotic factors and soil organic carbon stocks 36
4. Discussion 39
4.1. Magnitude and causes of edge effects on SOC stocks across urban and rural forests 39
4.2. Effects of anthropogenic activities on urban SOC stocks 40
5. Conclusion 42

Chapter 4. Spatial variations of soil organic carbon under diverse land cover types: application of laboratory-based hyperspectral reflectance spectroscopy 43
1. Introduction 43
2. Materials and Methods 44
2.1. Site description and Data collection 44
2.2. Data processing 45
2.3. Statistical analyses 46
3. Results and discussion 47
3.1. Spatial variations of SOC concentration and $\delta^{13}C$ among different land cover types 47
3.2. Assessments of urban SOC concentration using reflectance spectroscopy 49
4. Conclusions 50
References 52

Chapter 5. Conclusion 64

Abstract in Korean 66

List of Figures

Chapter 1

Figure 1.1 Evaluation of urban soil organic carbon (SOC) under three urbanization phenomena 5
Figure 1.2 Study flow.....7

Chapter 2

Figure 2.1 Locations of the study sites.....10
Figure 2.2 Vertical distribution of the soil bulk density (g cm^{-3}) and soil organic carbon (SOC) concentration (%) under impervious surfaces and vegetative surfaces 14
Figure 2.3 Vertical distribution of fine root mass density (g m^{-2}) beneath vegetative surfaces among three study sites 15
Figure 2.4 (a) Vertical profiles of soil organic carbon (SOC) stocks (kg m^{-2}) in three housing complexes. (b) Comparison of SOC at a depth of 5 m between impervious and vegetative surfaces.....16
Figure 2.5 Vertical distribution of soil ^{13}C and ^{15}N under (a) impervious surfaces and (b) vegetative surfaces.....17
Figure 2.6 Urbanization in southern Seoul (April, 1978) 20
Figure 2.7 Historical aerial photographs for land use change analysis at three housing complexes 20

Chapter 3

Figure 3.1 . Experimental design and setting using two-way transects....28
Figure 3.2. Representative view of the urban forest edges 29
Figure 3.3 SOC stocks (0-20 cm) along an urban-rural gradient from three fragmented urban forests to a large patch of rural forest.....34
Figure 3.4 Monthly variation in mean soil temperature (T_S) and volumetric water content (VWC) at a depth of 20 cm along an urban-rural gradient from urban forest to rural forest 35
Figure 3.5 Monthly differences in mean soil temperature (T_S) and volumetric water content (VWC) at a depth of 20 cm within urban forests 36
Figure 3.6 Relationship between SOC stocks (kgC m^{-2}) and ground-based biotic factors; fine root mass density and maximum leaf area index (2017-2018).....37
Figure 3.7 Annual litterfall mass (L_f) and SOC stocks along an urban-rural gradient 38
Figure 3.8 The spatial variation of the mean leaf area index (LAI) and the mean normalized difference vegetation index (NDVI) along an urban-rural gradient from urban to rural forests 40

Chapter 4

Figure 4.1 Soil organic carbon (SOC) concentration (%) with different land cover types.....50
Figure 4.2 Spatial variations of soil $\delta^{13}C$ among different land cover types. 51
Figure 4.3 Prediction scatter plot of soil organic carbon (SOC) concentration 53
Figure 4.4 Variable Importance in Projection (VIP) scores of optimized PLSR model 54

List of Tables

Chapter 3

Table 3.1 Description of sample plots, number of soil samples, mean elevation (m), mean slope angle (°), dominant plant species, and adjacent land use within two different forest types 30
Table 3.2 Relationship between mean SOC stocks (kgC m^{-2}) and topographic parameters (elevation and slope angle) based on 2017–2018 data from urban and rural forests. The transects are shown in Figure 1 36

Publications and Patent

Please note that some part of this dissertation proposal was written as stand-alone papers, patent (see below), and therefore there is some repetition in the methods and results.

1. Bae, J. & Ryu, Y. (2020) High soil organic carbon stocks under impervious surfaces contributed by urban deep cultural layers. *Landscape and Urban Planning*, 204, 103953.
2. Bae, J. & Ryu, Y. (2021) The magnitude and causes of edge effects on soil organic carbon stocks along an urban-rural gradient. *Landscape and Urban Planning*, (In major revision)
3. Republic of Korea, Patent 10-2020-0126777, "Method and structure for prediction system of spectral-based soil carbon, nitrogen, and their stable isotopes." September 29, 2020

Chapter 1. Introduction

1. Background

1.1. Urbanization and the cultural layers of SOC stocks

The amount of soil organic carbon (SOC) beneath impervious surfaces is important for assessing urban soil carbon budgets (Raciti et al., 2012; Yan et al., 2015). Soil sealing by impervious surfaces is one of the anthropogenic impacts on the spatial distribution of SOC (Edmondsonet et al., 2012; Lorenz & Lal, 2009). Impervious surfaces minimize carbon inputs by plants into soils (i.e., litter-fall and exudates via fine roots), so one might expect soils beneath impervious surfaces to be carbon-poor (Raciti et al., 2012; Yan et al., 2015). Indeed, a few studies have reported that soils beneath impervious surfaces had the lowest carbon storage capacity among the various urban land cover types (Wei et al., 2014a, Wei et al., 2014b). However, those studies have focused on the uppermost soil layer, which might miss the potential SOC in deep soils.

Urban soils record the history of urbanization, which involves land use and land cover changes that relocate SOC horizontally and vertically (Li et al., 2016; Lorenz & Lal, 2005). Intensive urbanization, and underground development in particular, leads to vertical heterogeneity of SOC (Pavao-Zuckerman, 2008). Previous studies reveal that some cities in Russia and South Korea have rich SOC in deeper layers, so called "cultural layers," which exist above or between the natural horizons in soils resulted from anthropogenic activities at different stages of development (Bae & Ryu, 2015; Mazurek et al., 2016; Vasenev et al., 2013). The magnitude and origin of deep SOC under different urban setting have not been well explored.

1.2. Edge effects on SOC stocks in fragmented urban landscape

Landscape fragmentation broadens the forest edge (Malmivaara-Lämsä et al., 2008; Pütz et al., 2014). Globally, 20% of forests are within 100 m of an edge, and more than 50% are within 500 m of an edge (Haddad et al., 2015). Many studies have addressed the impacts of forest fragmentation on habitat loss and species extinction in recent decades (Harris, 1988; Krauss et al., 2010). The potential impacts of forest fragmentation on soil organic carbon (SOC) stock changes within remnant forests, which determine regional carbon budgets, have recently received more attention (Barros & Fearnside, 2016; Smith et al., 2019).

Urban forests face diverse land use and socio-economic demands, which form complex, fragmented edges (Trlica et al., 2019). Urban expansion can result in forest fragmentation (Wade et al., 2003; Gong et al., 2013) or loss of surrounding soils (Bae & Ryu, 2020), but also influences urban forests and their management in a myriad of other ways. Urban forest edge effects involve diverse environmental parameters. Forest edges adjacent to non-planted or paved surfaces lead to a suite of unique and complex edge effects on the soil carbon cycle (Zheng et al., 2005). From the road edge to the forest interior, for example, urban forest edges differ in soil temperature and canopy height within the first 10 m (Delgado et al., 2007). The majority of SOC studies have been conducted in managed landscape (Pouyat et al., 2006; Bae & Ryu, 2015), but it remains unclear which anthropogenic factors influence the magnitude of the SOC stocks at urban forest edges (Bielinska et al., 2013).

1.3. City-scale assessments of SOC via hyperspectral data

Urbanization and land use change are accompanied by increasing anthropogenic pressure to soils (Herrmann et al., 2018). Urban soils are heterogeneous mixture of various parent materials and significantly affected by anthropogenic activities (Bae & Ryu, 2020). The natural source of soil organic carbon (SOC) is plant materials (Guo et al., 2007; Ladd et al., 2014), but urban materials provide an

additional source of SOC in urban area (Guo et al., 2013). Tracing the source of SOC in diverse land use pattern is important for assessing the consequences of urbanization on urban SOC budgets. The relationship between SOC change and human activities, however, is primarily focused on agricultural and forest soils.

Understanding the consequences of human activities on SOC is increasingly important with the expanding urban land area (Vasenev & Kuzyakov, 2018). Improving our understanding of the relationships between the pattern of land use and the SOC stocks requires large amounts of timely and cost efficient SOC analysis, which is difficult to obtain with routine chemical analysis. To manage SOC budgets at the city scale, there is an urgent need to qualify both SOC stocks and their sources (Guo et al., 2017; Rogers et al., 2017). Stable carbon isotopes are considered as an invaluable tool for monitoring SOC, both as a tracer and as a record of processes in which isotopic fractionation occurs (Bowling et al., 2008). Extensive soil sampling is required at city scale to accurately estimate the SOC and the carbon isotopic composition (expressed as $\delta^{13}C$), however, it is an expensive and time-consuming process. Therefore, a rapid and cost-effective alternative method to quantify SOC with acceptable precision, is needed.

2. Purpose

In this dissertation, I aimed to find the spatial and vertical variations of soil organic carbon (SOC) stocks under three urbanization phenomena (Figure 1.1).

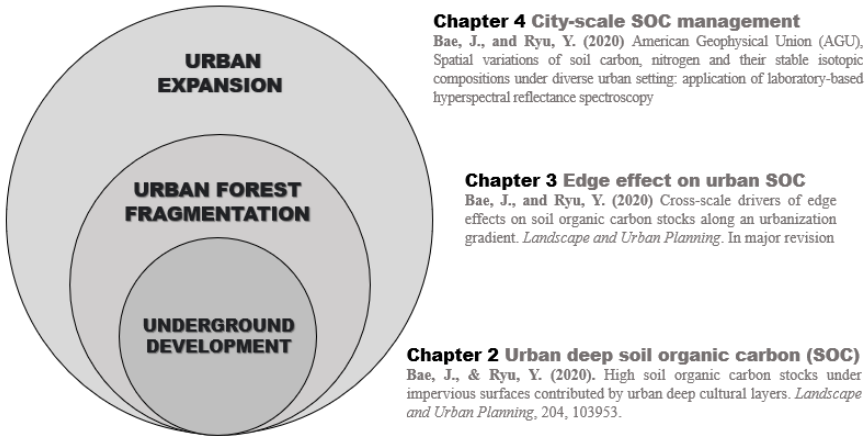

Figure 1.1 Evaluation of urban soil organic carbon (SOC) under three urbanization phenomena.

In Chapter 2, I quantified SOC stocks to a 5 m depth beneath impervious surfaces and adjacent vegetative surfaces at three housing complexes in Seoul, Republic of Korea. The objectives were (1) to quantify the spatial and vertical distribution of SOC stocks beneath impervious surfaces and vegetative surfaces; (2) to investigate the key factors that control the spatial and vertical distribution of SOC stocks; and (3) to understand how anthropogenic factors affect SOC stocks in heterogeneous urban setting.

In Chapter 3, I quantified the edge effects on SOC stocks along an urban–rural gradient from three fragmented urban forests to a large patch of rural forest. The objectives were to (1) quantify edge effects on SOC stocks along an urban–rural gradient; (2) investigate which factors control edge effects on SOC stocks between fragmented urban forests and the rural forest; and (3) understand how surrounding land uses affect edge effects on SOC stocks within the urban forests.

In Chapter 4, I investigated the spatial variations of soil organic carbon (SOC) and $\delta^{13}C$ values among six land cover types in an urban park. I took hyperspectral reflectance for each soil sample using ASD–FieldSpec after drying and removing stones (> 2 mm

diameter), then used partial least squares (PLS) regression to establish the predictive models for SOC and $\delta^{13}C$ values in urban soils. Specific objectives of this study include: 1) to quantify the spatial variations of SOC and $\delta^{13}C$ among different land cover; 2) to assess the potential for spectroscopy to predict for SOC under heterogeneous land cover types.

.

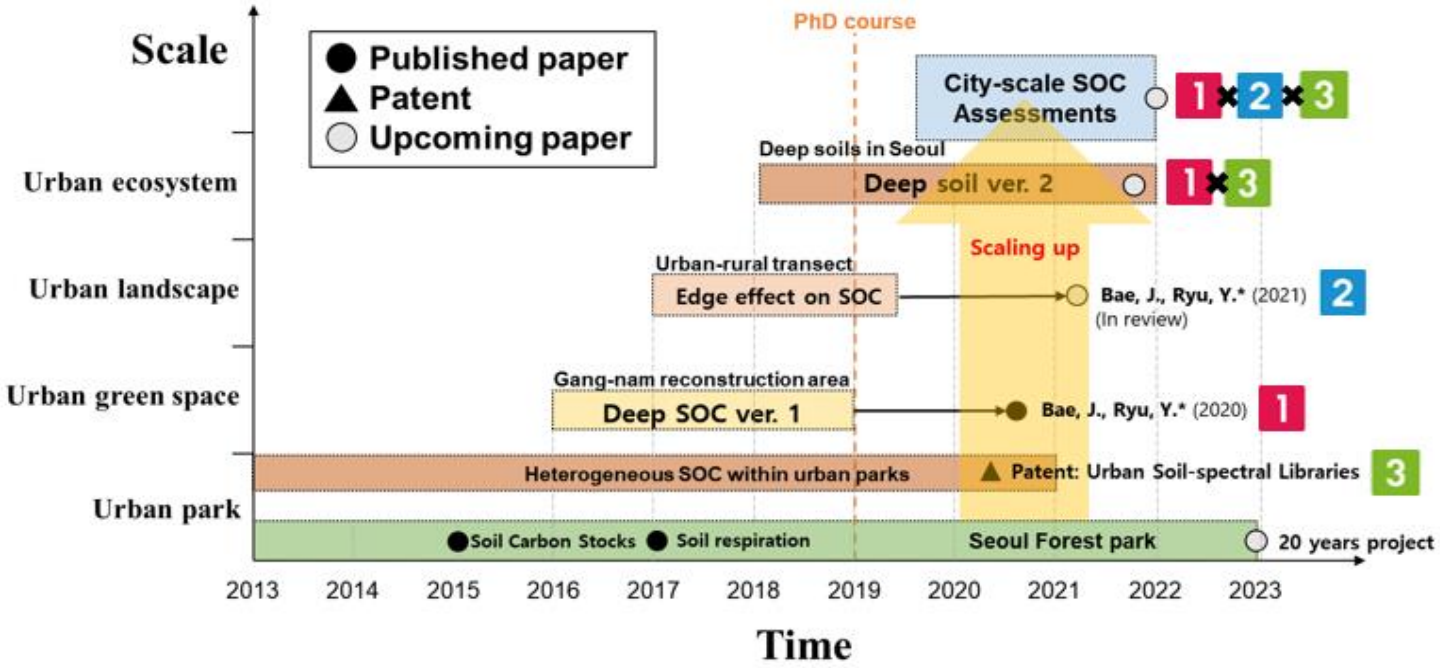

Figure 1.2 Study flow

Chapter 2: High soil organic carbon stocks under impervious surfaces contributed by urban deep cultural layers

1. Introduction

Expansion of impervious surface is an outward sign of urbanization (Churkina, 2008). Impervious surfaces support human mobility and urban infrastructure, and cover a large fraction of land in urban settings (Elvidge et al., 2007; Scalenghe & Marsan, 2009). Globally, constructed impervious surfaces covered more than 579,000 km^2 in the early 2000s (Elvidge et al., 2007). The mean sealed area of 38 European cities was around 48% (Scalenghe & Marsan, 2009). Estimates of impervious surface area among seven U.S. cities ranged from 40% to 60% (Nowak et al., 1996; Pouyat et al., 2006). In 48 Asian countries, impervious surface area accounted for more than 64% of total urban area (Kuang et al., 2016). Extensive studies of the negative effects of impervious surfaces on storm water runoff and urban heat islands have been conducted (Yuan & Bauer 2007, Miller et al., 2014); however, few studies have addressed the roles of impervious surfaces in quantifying urban soil carbon budgets.

The amount of soil organic carbon (SOC) beneath impervious surfaces is important for assessing urban soil carbon budgets (Raciti et al., 2012; Yan et al., 2015). Soil sealing by impervious surfaces is one of the anthropogenic impacts on the spatial distribution of SOC (Lorenz & Lal, 2009; Edmondson et al., 2012). Impervious surfaces minimize carbon inputs by plants into soils (i.e., litter-fall and exudates via fine roots), so one might expect soils beneath impervious surfaces to be carbon-poor (Raciti et al., 2012; Yan et al., 2015). Indeed, a few studies have reported that soils beneath impervious surfaces had the lowest carbon storage capacity among the various urban land cover types (Wei et al., 2014a; Wei et al.,

2014b). However, those studies have focused on the uppermost soil layer, which might miss the potential SOC in deep soils.

Urban soils record the history of urbanization, which involves land use and land cover changes that relocate SOC horizontally and vertically (Lorenz & Lal 2005; Li et al., 2016). Intensive urbanization, and underground development in particular, leads to vertical heterogeneity of SOC (Pavao-Zuckerman, 2008). Previous studies reveal that some cities in Russia and South Korea have rich SOC in deeper layers, so-called "cultural layers," which exist above or between the natural horizons in soils resulted from anthropogenic activities at different stages of development (Vasenev et al., 2013; Bae & Ryu, 2015; Mazurek et al., 2016). The magnitude and origin of deep SOC under different urban setting have not been well explored.

In this study, we analyze soil samples to a 5 m depth beneath impervious surfaces and adjacent vegetative surfaces at three housing complexes in Seoul, Republic of Korea. We also quantify the vertical distribution of soil ^{13}C and ^{15}N in the upper 5 m of soil to infer the origins of the SOC. The objectives of this study were (1) to quantify the vertical distribution of SOC stocks (to a depth of 5 m) beneath impervious surfaces and vegetative surfaces; (2) to investigate the key factors that control the vertical distribution of SOC stocks; and (3) to understand the effects of impervious surfaces on SOC stocks in an urban area.

2. Methods and materials

2.1 Site description

This study was conducted in three residential areas, housing complexes in the Seo-cho and Gang-nam districts, Seoul, Republic of Korea (Fig. 2.1). The three housing complexes are located within a 6 km radius. Detailed site descriptions are shown in Table 1. The study sites are located in a temperate monsoon climate with a mean annual temperature of 12.5℃ and mean annual precipitation of 1,450 mm (Korean Meteorological Administration). Sites A and B are flat and have an elevation of approximately 15 m, while Site C has an average elevation of 25 m, with a height difference of 15 m in the

north–south direction (Google Earth ver. 7.1.2.2041). The geological characteristics consists of granitic gneisses (Site C) and quaternary alluvial layers around the Han River (Sites A and B) (Yun et al., 2007).

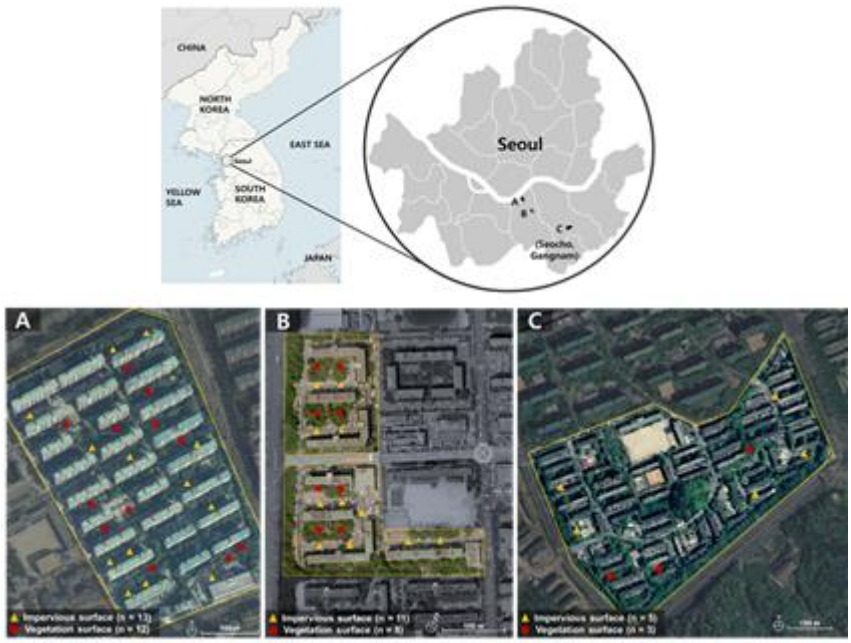

Figure 2.1 Locations of the study sites: housing complexes A, B and C. The soil sampling locations are marked by triangles (impervious surfaces) and circles (vegetative surfaces). The location of the soil sampling was determined based on construction points under the geological survey for the formal reconstruction plan in each study site.

The housing complexes were built in the late 1970s to early 1980s, and surfaces have been in place for roughly 40 years. In all three sites, litter–fall on the vegetative surfaces are preserved, while litter–fall on the impervious surface are artificially relocated to the adjacent vegetative surfaces. Reconstruction of those housing complexes by 2021 after complete demolition is planned. Korea Land and Housing Corporation guidelines require collecting deep soil samples at the areas where new housing complexes will be built. This guideline offers an unintended opportunity for us to access deep soil samples in currently both impervious and vegetative surfaces. Historical aerial photographs taken in the mid–1970s to early 1980s

provided by the Seoul Metropolitan Government were used to characterize land use changes from before construction of the housing complexes.

2.2. Data collection

Soil samples were collected in June 2017 (Site A), October 2016 (Site B), and July 2018 (Site C). Three local construction companies chose the detailed sampling locations based on the guideline of Korea Land and Housing Corporation, which require deep soil and bedrock samples at 0.5–1.0 m interval where new buildings will be constructed. It allowed us to get soil samples from 25 (13 and 12 for impervious and vegetative), 19 (11 and 8 for impervious and vegetative), and 8 (5 and 3 for impervious and vegetative) points at Sites A, B, and C, respectively (Fig. 2.1). We estimated SOC stocks to a depth of 5 m under impervious surfaces and adjacent vegetative surfaces. Concrete pavement and surface litter were removed before soil sampling. Then, we collected seven soil samples along the vertical soil profile (0–0.2, 0.2–0.5, 0.5–1.0, 1.0–2.0, 2.0–3.0, 3.0–4.0, and 4.0–5.0 m) using a portable soil boring machine (KW180; Zhejiang, China). To avoid artificial disturbance during soil boring, except when removing concrete pavement, all soil samples were collected using undisturbed soil cores (5.5 cm inner diameter, 70 cm length) with a vertical hammering process in each target depth interval.

2.3. Data processing

To quantify SOC stocks, the soil samples were oven-dried (C-DH; Chang Shin Scientific Co., Pusan, Korea) at 105℃ for two days in the laboratory (USDA-NRCS 1992) and then strained through a 2 mm standard testing sieve (Chung Gye Sang Gong SA, Seoul, Korea) to remove stones. The soil bulk density at each depth interval was determined using the following equation (Adams, 1973):

$$\text{Soil bulk density} = \frac{(total\ dry\ mass - rock\ mass)}{(total\ volume - rock\ volume} \quad (1)$$

To estimate the rock volume from the rock mass, we used a standard rock particle density, 2.65 Mg m^{-3} (Brady & Weil, 2007).

To remove any inorganic carbon within the soil sample (Edmondson et al., 2015), 10 mL HCI (5.7 M) was added to 2.5 g of each soil sample and the soil samples dried at 105℃ for 24 h. SOC concentration was quantified using an Elemental Analyzer (Flash EA 1112; Thermo Electron, Waltham, MA, USA) at the National Instrumentation Center for Environmental Management (NICEM). To measure fine root mass density, we separated living fine roots (<2 mm diameter) from the soils with tweezers, washed the fine roots, and oven-dried them at 70℃ for two days (Olsthoorn 1991). The isotopic compositions (expressed as ^{13}C and ^{15}N) were measured in the topsoil (0–0.2 m), subsoils (1.0–2.0 m for impervious surfaces and 2.0–3.0 m for vegetative surfaces), and in the bottom layer (4.0–5.0 m depth). Both ^{13}C and ^{15}N were determined with continuous-flow isotope ratio mass spectrometry (OPTIMA, Micromass, UK Ltd) at the NICEM. Carbon isotope ratio (^{13}C) is calculated using the following equation (Farquhar et al., 1989):

$$\delta\,13C = \left\{ \frac{\left(\frac{13C}{12C}\right)sample}{\left(\frac{13C}{12C}\right)standard} - 1 \right\} \times 1000 \qquad (2)$$

where the standard is the ratio of PDB (Pee Dee Belemnite). A similar equation applies for 15N, for which the standard is that of atmospheric nitrogen (Mariotti, 1983). Soil texture was classified using the percentages of sand, silt, and clay as determined by the hydrometer method (Gee and Bauder, 1979). The textural classes were determined based on the USDA soil classification scheme (USDA 2010).

2.4. Statistical analyses

All statistical analyses were performed using SigmaPlot 12.0 (Systat Software, Inc., Chicago, IL, USA). Analysis of variance (ANOVA) was used, followed by Tukey's post hoc test, to test

differences in soil bulk density, SOC concentration, SOC stocks, ^{13}C, and ^{15}N among soil depth intervals for each land use. We also used Student's t-test to compare all soil data from each depth interval between impervious surface and vegetative surface. All data are presented as the mean ± 95% CI, unless otherwise specified.

3. Results

3.1. Vertical distributions of soil bulk density, SOC concentration and fine roots

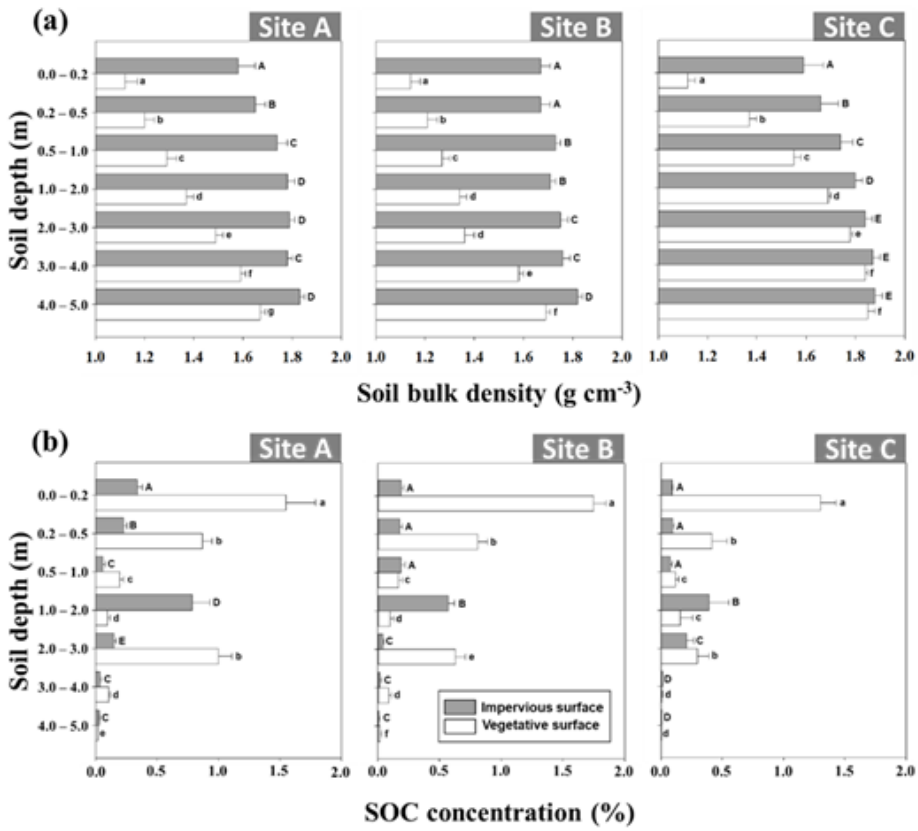

Figure 2.2 (a) Vertical distribution of the soil bulk density (g cm^{-3}) and (b) soil organic carbon (SOC) concentration (%) under impervious surfaces and vegetative surfaces. The different letters indicate significant differences among the soil depth intervals (Tukey test, $P < 0.05$); capital and lower-case letters indicate soils under impervious and vegetative surfaces, respectively. Error bars indicate 95% CI.

The soil bulk density beneath vegetative surface increased with soil depth from 1.12 to 1.85 g cm^{-3}, with the highest soil bulk density in the bottom layer (4.0–5.0 m depth: Fig. 2.2a). In impervious area, the range of soil bulk density with increasing soil depth was narrowed to 1.58 to 1.88 g cm^{-3}. When compared with the soil samples taken from different depth intervals, the soil bulk density beneath impervious surface is higher than that of vegetative surface (t−test, $P < 0.05$), except at 3.0–5.0 m depth in Site C. The highest SOC concentration beneath vegetative surface was located at the topsoil (0–0.2 m depth) in all of the study sites ($P < 0.05$, Fig 2.2b), whereas in impervious surface, the highest SOC concentration located at 1.0–2.0 m soil depth ($P < 0.05$, Fig 2.2b). In the top 1 m of the profile, the SOC concentration beneath vegetative surface decreased steadily with soil depth at all of the study sites (ANOVA, $P < 0.05$).

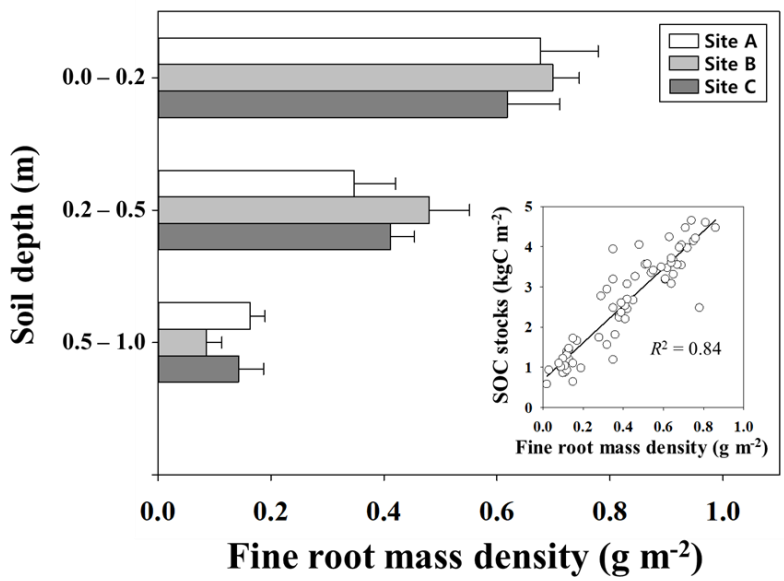

Figure 2.3 Vertical distribution of fine root mass density (g m^{-2}) beneath vegetative surfaces among three study sites. Error bars indicate 95% CI. The correlation between fine root mass density and soil organic carbon (SOC) stocks (kg m^{-2}) beneath vegetation surfaces is presented in the inset graph.

Figure 2.3 shows the vertical distribution of fine root mass density (g m^{-2}) beneath vegetative surfaces in all study sites. More than 96% of the fine root mass density appeared within 1 m of soil depth. The fine root mass density decreased with soil depth in all study sites. There was a significant relationship between fine root

mass density and SOC stocks among three study sites (R^2 = 0.84, see inset in Fig. 2.3).

3.2. Vertical distribution of SOC stocks

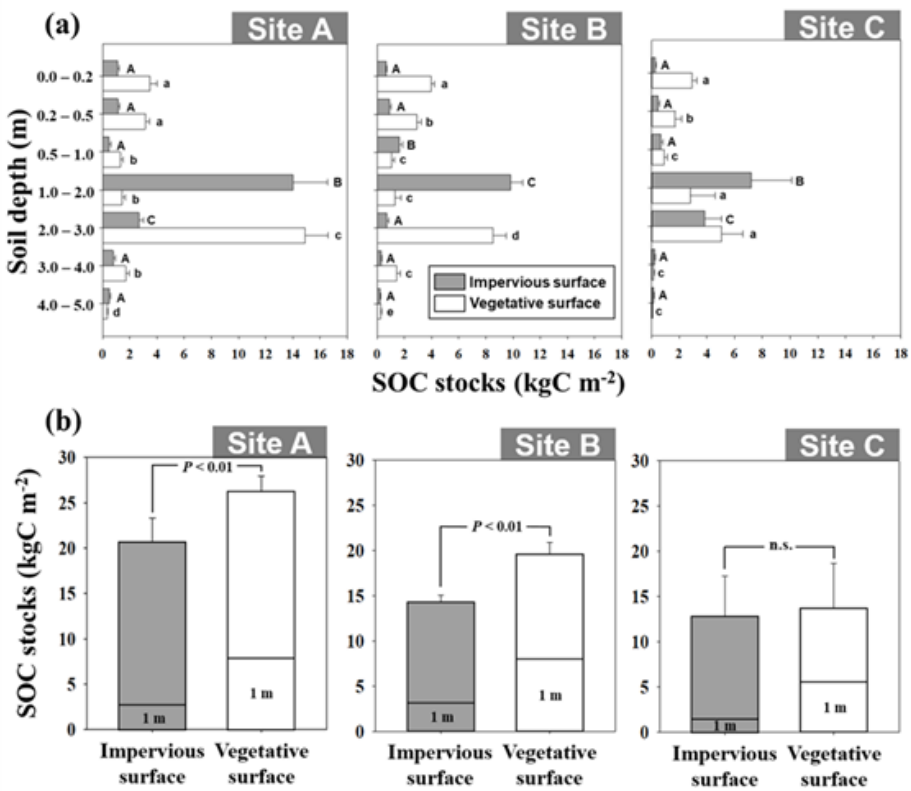

Figure 2.4 (a) Vertical profiles of soil organic carbon (SOC) stocks (kg m^{-2}) in three housing complexes. (b) Comparison of SOC at a depth of 5 m between impervious and vegetative surfaces. The different letters indicate significant differences in SOC among the soil depth intervals (ANOVA, $P < 0.05$); capital and lowercase letters indicate soils under impervious and vegetative surfaces, respectively. Error bars indicate 95% CI.

We found a sharp increase in SOC stocks at depths of 1.0–3.0 m beneath both surfaces at all three sites (Fig. 2.4a). The highest SOC stocks at subsoil layers (1.0–3.0 m) create an abrupt soil boundary and contain substantial amounts of SOC, which account for >68% of SOC stocks to a depth of 5 m. The proportions of SOC stocks at depths of 1 m to 5 m were 16% beneath impervious surfaces and 34% beneath vegetative surfaces. Thus, SOC stocks to a 5 m depth were comparable between impervious surfaces (16.9 ± 1.9 kgC m^{-2}) and

vegetative surfaces (22.3 ± 2.2 kgC m^{-2}) (Fig. 2.4b). At Sites A and B, SOC stocks beneath impervious surfaces were around 75 to 80% of those under vegetative surfaces, while there was no significant difference in SOC stocks between the two surfaces at Site C. In Site C, high SOC stocks under 1 m depth appeared more broadly compared to the other two sites.

3.3. Depth profiles of soil carbon and nitrogen isotopes

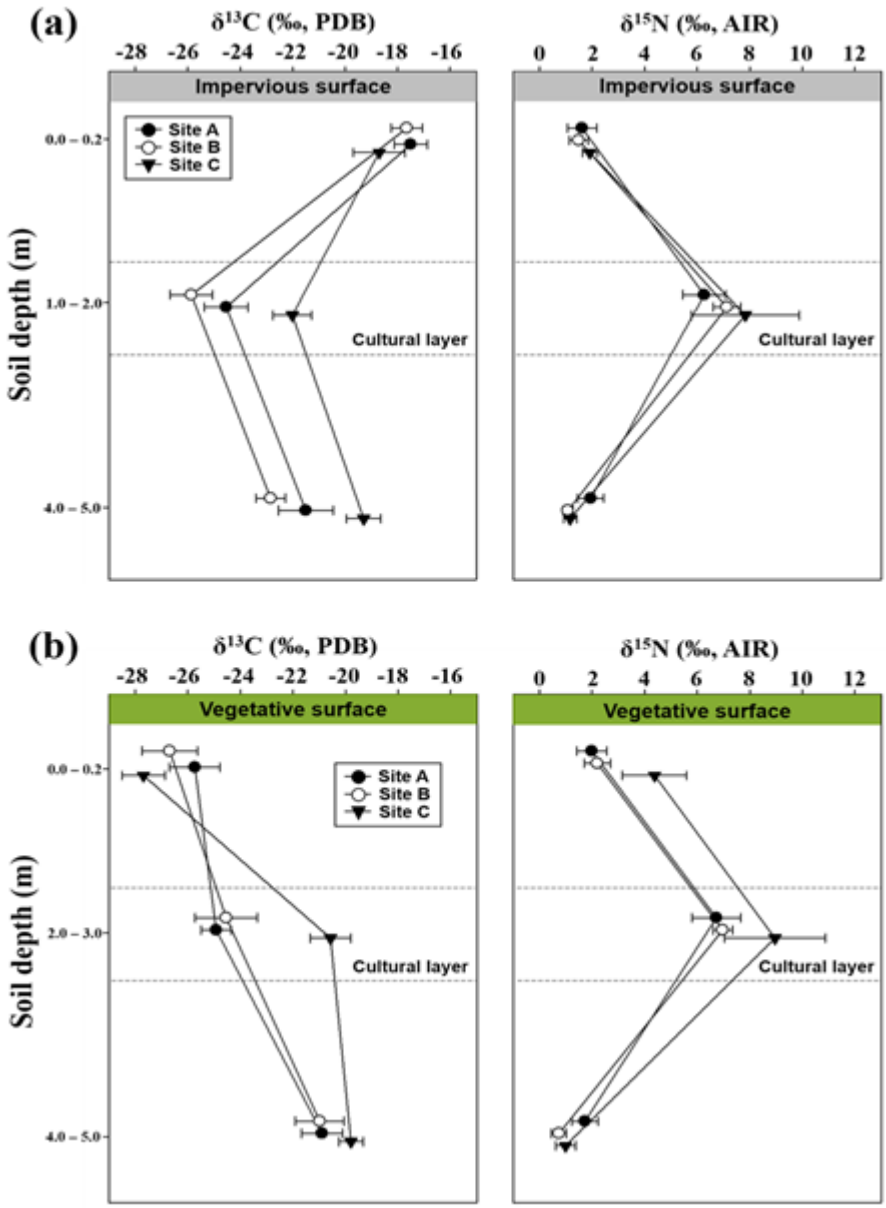

Figure 2.5 Vertical distribution of soil ^{13}C and ^{15}N under (a) impervious surfaces and (b) vegetative surfaces. Plot points were jittered along the y-axis to avoid overlap of error bars. Error bars indicate 95% CI.

There were significant differences between impervious and vegetative surfaces in terms of ^{13}C in the topsoil (0–0.2 m) at all three sites (t-test, $P < 0.05$) (Fig. 2.5). The topsoil ^{13}C values beneath impervious surfaces (−17.8 ± 0.4‰) were more enriched (less negative) than those under vegetative surfaces (−26.3 ± 0.7‰). In vegetative areas, the ^{13}C values at the bottom layer (4.0–5.0 m depth) are more enriched (less negative) than topsoil layer (Fig. 2.5b), whereas in impervious area, the most enriched soil ^{13}C values were found in topsoil (Fig. 2.5a). Soil ^{15}N values at the cultural layers (1.0–3.0 m) significantly larger than those for topsoil layer (0–0.2 m) and bottom layer (4.0–5.0 m), regardless of their surface type. We found no significant difference in soil ^{13}C or ^{15}N in the cultural layers between impervious surfaces and vegetative surfaces (t-test, $P > 0.05$), except for ^{13}C values at Site C (P-value = 0.048).

4. Discussion

4.1 What controls vertical heterogeneity of urban SOC stocks?

Land cover types mainly contributed to spatio-vertical heterogeneity of SOC stocks. We found a three-fold difference in SOC stocks in the top 1 m between impervious surfaces (2.7 ± 0.3 kgC m^{-2}) and vegetative surfaces (7.6 ± 0.6 kgC m^{-2}) (Fig. 2.4b). The stark difference might be related to SOC accumulation via plant production over the last 40 years in the vegetative surfaces. A previous study in the same city reported that SOC stocks in vegetative surfaces (7.3–10.2 kgC m^{-2}) were four times greater than non-vegetated surfaces (1.6 ± 0.1 kgC m^{-2}) (Bae & Ryu, 2015). Fine root residues, originated from plant production, are the main input source of SOC (Guo et al., 2007), which could be correlated with the vertical distribution of urban SOC stocks (Bae & Ryu, 2015). Indeed, fine roots biomass in this study were mainly distributed within 1 m of soil depth (>96%), and the linear relationship between

fine root mass density and SOC stocks was also high (R^2 = 0.84) among three study sites (see inset in Fig. 2.3).

Land use pattern is a potential determinant for vertical heterogeneity of SOC stocks. In this study, the largest SOC stocks beneath both surfaces were distributed in deep soil layers. We found rich SOC stocks at depths of 1.0–3.0 m, with more than 78% beneath impervious surfaces and more than 56% beneath vegetative surfaces compared to the total SOC stocks to a 5 m depth. Our results show that the amount of SOC stocks in deep soil layers (1.0–3.0 m) between impervious surface (13.4 ± 1.8 kgC m^{-2}) and vegetative surface (13.0 ± 1.8 kgC m^{-2}) were comparable. The three housing complexes were built in similar period from 1978–1982, and they are located within a 6 km distance. Furthermore, soil ^{13}C and ^{15}N in the deep soil layers between two surfaces were not significantly different (Fig 2.5). For these reasons, we assume that deep SOC stocks in our sites may be linked to past urbanization processes.

The soil ^{15}N data indicates that high SOC stocks in the deep soil layer stemmed from agricultural soils, which was the land use before the housing complexes were built. The soil ^{15}N values in the deep soil layer (7.0 ± 0.4‰) were significantly higher than those in the other soil layers and were similar to the typical ranges of agricultural soils (5 to 20‰) (Norra et al., 2005). The soil ^{15}N values are tightly associated with land use patterns (Boeckx et al., 2006). The main source of N in urban areas is atmospheric NOX deposition, which leads to soil ^{15}N near 2‰ (Fang et al., 2011), as seen in the topsoil ^{15}N values beneath vegetative surfaces (Fig. 2.5b). Therefore, the high values of soil ^{15}N in the deep soil layers are likely linked to past agricultural activities including use of organic fertilizers (Bateman & Kelly, 2007; Thornton et al., 2015).

Figure 2.6 Urbanization in southern Seoul (April, 1978). This photograph shows the land use change from cropland to urban housing complexes in the late 1970s. The location of the photograph is within 5 km of all the study sites. The copyright of the photograph is held by the documentary photographer, Min-Cho Jun.

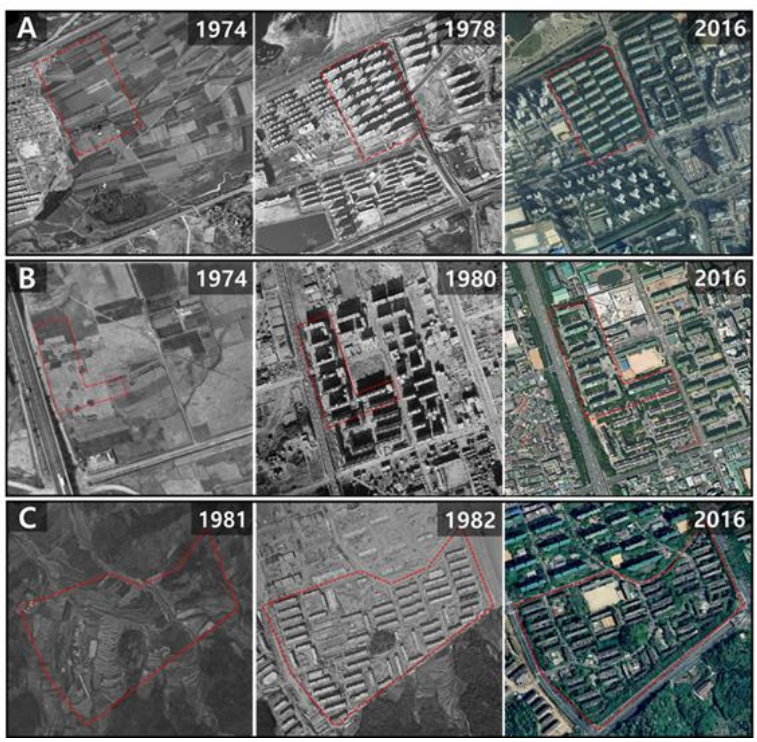

Figure 2.7 Historical aerial photographs for land use change analysis at three housing complexes. All residential areas (housing complexes) were used as agricultural land until the 1970s. Red dashed lines indicate the boundary of each residential area. All photographs were obtained from the Aerogis database from the Seoul metropolitan government.

The agricultural area in south of Seoul has experienced expansive land use changes since the early 1970s (Kim et al., 2003). They include rapid urbanization and a significant loss of agricultural land to residential development (Fig. 2.6). We used aerial photographs across study sites to understand how vertical profiles of soil ^{13}C and ^{15}N were influenced by site-specific land use history. Our three sites were used for rice paddies (Sites A and B: flooded rice paddy, Site C: terraced rice paddy) until the mid-1970s and were then developed into housing complexes (Fig. 2.7). While modern agricultural soils mostly receive chemical fertilizers having a near-zero ^{15}N (−2‰ to 2‰) (Rogers et al., 2017), organic fertilizers such as animal manure have relatively high ^{15}N values, with wide ranges of 8.5‰ to 12.9‰ (Bateman & Kelly, 2007; Stevenson et al., 2010). Historical information on the type of fertilizer used at each sampling point is not directly available, but we assume that organic fertilizers such as raw manure were used primarily until the mid-1970s rather than chemical fertilizer (Lee & Kim, 2009), as evidenced by the photo taken nearby the Sites A and B (Fig. 2.6).

Furthermore, we believe that thicker cultural layers in Site C than the other sites (Fig 2.4a) may be explained by differences of former cultivated systems. As mentioned in the Method, Site C has a height difference of 15 m in the north-south direction. Topographic aspects of agricultural fields and their interactions with management should be taken into account when estimating SOC stock changes (Hbirkou et al., 2012). Figure 2.7 shows the land use patterns and previous cultivated systems among three study sites. Site C was a terraced farmland that has been cut into a series of successively receding flat surfaces. Our results, therefore, suggest that soil burial, mixing, and cut-and-fill processes performed during conversion of agricultural areas to residential areas created thicker cultural layers.

4.2. How does the impervious surfaces affect the urban SOC stocks?

High soil bulk density beneath impervious surface led to a heterogeneous vertical distribution of SOC stock. Soil bulk density

beneath impervious surfaces (>1.6 g cm^{-3}) was significantly higher than vegetative surfaces (>1.1 g cm^{-3}) at most soil layers (Fig. 2.2a). The SOC concentration beneath both surfaces decreased with soil depth until reaching the cultural layers (Fig. 2.2b), but at Sites B and C, the SOC stocks beneath impervious surface increased (Fig. 2.4a) due to the high soil bulk density. In this study, high values of soil bulk density were consistent with the previous urban study that reported higher soil bulk density beneath impervious surfaces (Yan et al. 2015), ranging 1.4 to 1.8 g cm^{-3}. Soil compaction and sealing can cause reduced SOC capacity and nutrient imbalances in urban soils (Raciti et al., 2012), which can greatly limit soil enzyme activities and root growth of surrounding vegetation (Viswanathan et al., 2011). In our study, the mean SOC stocks at the top 0.2 m (0.78 kgC m^{-2}) beneath impervious surfaces are lower than that found in New York City (2.29 kgC m^{-2}) (Edmondson et al., 2012; Raciti et al., 2012). The lower SOC stocks in the topsoil layer might be related to the lower clay contents in our site (< 8%) and coarser soil texture, which could lead to lower SOC capacity.

The stable carbon isotopic composition of the topsoil revealed the origins of SOC. Previous study reported that soil ^{13}C values in urban area are related to the constituent carbon source such as building materials and road surfaces (Kvenvolden et al., 1998). Concrete materials have ^{13}C values from −8.0‰ to −17.5‰ (Norra et al., 2005; Schleicher et al., 2013), comparable to those in the topsoil beneath impervious surfaces (Fig 2.5a). This implies that the topsoil beneath impervious surfaces are likely mixed with or influenced by the concrete particles, resulting in more heterogeneous vertical distributions of ^{13}C. Meanwhile, the most depleted ^{13}C values within vegetative surfaces were found in the topsoil layer (Fig 2.5b).

The vertical profile of soil ^{13}C in vegetative surface was enriched (less negative) with increasing soil depths. Since the Industrial Revolution, anthropogenic burning of fossil fuels with low ^{13}C led to a decrease in atmospheric $^{13}C-CO_2$, which also caused the ^{13}C of plant biomass and soil to decrease in urbanized areas (Wang et al., 2017). This so-called "Suess effect" could be partly responsible

for the observed depletion of ^{13}C in the topsoil layer (Revelle & Suess, 1957). Meanwhile, the range of ^{13}C in topsoil beneath vegetative surfaces (−27‰ to −25‰) is consistent with urban forest soils under C3 plants (−26‰ to −24‰) in the Asian monsoon climate (Guo et al., 2013; Guo et al., 2017).

4.3. How can deep SOC data be used for sustainable urban development?

Understanding the present and future distribution of SOC is critical to supporting carbon budget assessments. To understand cause and magnitude of rich SOC stocks in deep soils are important for evaluating urban carbon budgets. Rapid urbanization around the world has encroached on agricultural areas (Hara et al., 2005; Wu et al., 2006). Rich SOC stocks in the agricultural areas likely remain under urban surfaces, resulting in unintentional carbon capture and storage. Therefore, counting carbon stored in urban regions must consider deeper soils (Lorenz & Lal 2005; Lorenz & Lal 2009), which cannot be achieved with conventional soil sampling at 1 m depth (Yost & Hartemink, 2020).

High SOC stocks in deep soil layers are less studied than topsoil layer, but are also under threat from human disturbance. Long−term stabilization of SOC stocks at deep soil layers is adequately explained by the slow turnover times under anaerobic conditions (Torn et al., 1997; Salome et al., 2010; Rumpel & Kogel−Knabner, 2011) with a high rate of clay contents in cultural layers, which protect SOC against microbial decomposition (Chaopricha & Marin−Spiotta, 2014).

Rich SOC stocks in deep cultural layers may be vulnerable to vertical disturbances from future constructions. The limited urban area promotes underground development. In the world ' s increasingly populated regions, urban planners and policy makers are building down as well as up (Broere, 2016). These inevitable development trends will disturb the deep soil profile and at the same time translocate the deep soils to the land surface (Herrmann et al., 2018). A sudden shift from anaerobic to aerobic conditions may lead to a dramatic increase in SOC decomposition (Keiluweit et al., 2017),

especially in cities with warmer surface temperature (Lee et al., 2015; Bae & Ryu, 2017). In fact, in Site C, a total volume of 1,588,900 m^3 of soils (4 m soil depths) will be dug up from 2020 to develop underground parking lots. If we do not trace these anthropogenic SOC translocations under future urban constructions, we could not effectively design and implement strategies to monitor urban carbon cycles.

The outcomes of this study could help urban planners and policy makers. Underground developments which appear in many places in cities generate large amounts of excavated deep soils. It is common to transport those soils outside of the city which increase carbon footprint. If high, deep SOC are found like the case in this study, it will be desirable to reuse the soils for the needs nearby the construction site such as soil amendments, planting trees and making urban parks. Recycling the deep SOC within the city will reduce carbon footprint and economic costs (Magnusson et al., 2015).

Consequently, it is imperative to generate urban SOC maps that include cultural layers beneath both pervious and impervious surfaces, which could help urban planning and development while managing urban SOC stocks.

5. Conclusions

Our results showed that deep soils are hidden elements of the carbon budget in the urban region. We provided evidence that land use changes can lead to long-lasting effects on vertical heterogeneity of SOC stocks in urban areas. The magnitude of SOC stocks varied with land cover types and origins of SOC depended on the soil depths, which reflected the land use history. Our results highlight that deep soils under impervious surfaces could be overlooked carbon hotspots in urban ecosystems. More attention must be given to soils under impervious surfaces, which have been largely ignored in urban carbon budgets. We call more efforts to understand the deep SOC change mechanisms with urbanization across various spatial and temporal scales.

Chapter 3: The magnitude and causes of edge effects on soil organic carbon stocks along an urban–rural gradient

1. Introduction

Landscape fragmentation broadens the forest edge (Malmivaara–Lämsä et al., 2008; Pütz et al., 2014). Globally, 20% of forests are within 100 m of an edge, and more than 50% are within 500 m of an edge (Haddad et al., 2015). Many studies have addressed the impacts of forest fragmentation on habitat loss and species extinction in recent decades (Harris 1988; Krauss et al., 2010). The potential impacts of forest fragmentation on soil organic carbon (SOC) stock changes within remnant forests, which determine regional carbon budgets, have recently received more attention (Barros & Fearnside, 2016; Smith et al., 2019).

Forest edges are due to the natural disturbance or anthropogenic activities and gradually affect both abiotic and biotic factors. This phenomenon, known as the "edge effect", is commonly defined as a difference in bioclimatic factors that exist along the forest edges relative to the forest interiors. Microclimatic gradients between the forest interior and its edge (Camargo & Kapos, 1995; Gehlhausen et al., 2000) affect plant carbon assimilation and SOC turnover rates (Barros & Fearnside 2016; Reinmann & Hutyra, 2017). Recent studies have reported changes in the forest edge microclimate, such as increased air temperature, soil drying, incidence of light and wind, and decreased above–ground biomass and SOC pools (Ruwanza, 2019; Smith et al., 2019). In tropical forests, the annual litterfall mass within 10 m of the edge was significantly lower than its interior (Sizer et al., 2000), and above–ground biomass within 500 m of the forest edge was 25% lower than the forest interior (Chaplin–Kramer et al., 2015). Two major pathways for carbon input into soils include litterfall and exudates via fine roots (diameter < 2.0 mm) (Riutta et al., 2016). Thus, changes in the plant productivity of forest edges underpin the edge effect on SOC stocks (Barros & Fearnside, 2016).

However, the causes and magnitude of edge effects on SOC

stocks between urban and rural forests have been less well characterized.

Urban forests face diverse land use and socio-economic demands, which form complex, fragmented edges (Trlica et al., 2019). Urban expansion can result in forest fragmentation (Wade et al., 2003; Gong et al., 2013) or loss of surrounding soils (Bae & Ryu, 2020), but also influences urban forests and their management in a myriad of other ways. Urban forest edge effects involve diverse environmental parameters. Forest edges adjacent to non-planted or paved surfaces lead to a suite of unique and complex edge effects on the soil carbon cycle (Zheng et al., 2005). From the road edge to the forest interior, for example, urban forest edges differ in soil temperature and canopy height within the first 10 m (Delgado et al., 2007). The majority of SOC studies have been conducted in managed landscape (Pouyat et al., 2006; Bae & Ryu, 2015), but it remains unclear which anthropogenic factors influence the magnitude of the SOC stocks at urban forest edges (Bielinska et al., 2013).

Assessments that focus only on the abiotic or biotic factors of edge effects on urban SOC stocks can lead to controversial results (Malmivaara-Lämsä et al., 2008; Hamberg et al., 2009). Urban forest edges are vulnerable to SOC loss due to wind and water erosion; the breakdown of soil aggregates is mainly caused by human activities (Lorenz & Lal, 2009). Previous studies indicate that SOC content in urban forest edges is 30% to 45% lower than in forest interiors (Malmivaara-Lämsä et al., 2008), due to a low moisture content of the humus near the edge. By contrast, some urban SOC stocks in hardwood-dominant forest edges are similar to or higher than those in forest interiors (Hamberg et al., 2009; Reinmann & Hutyra, 2017) due to enhanced plant growth under increased light and water supplies. Thus, one of the challenges for quantifying carbon budgets in urban forests is to quantify accurately how multiple, simultaneous, and ongoing human activities that alter biotic and abiotic factors affect the magnitude of SOC stocks in forest edges.

In this study, our objectives were to (1) quantify edge effects on SOC stocks along an urban-rural gradient; (2) investigate which

factors control edge effects on SOC stocks between fragmented urban forests and the rural forest; and (3) understand how surrounding land uses affect edge effects on SOC stocks within the urban forests. To identify the magnitude and causes of the edge effects on SOC stocks, we quantified the SOC stocks and environmental factors along an urban–rural gradient from using linear, parallel transects at 100 m intervals. To determine if surrounding land use could explain diverse edge effects within urban forests, we simultaneously measured the SOC stocks in plot scale (at 20 m intervals).

2. Methods and Materials

2.1. Site description

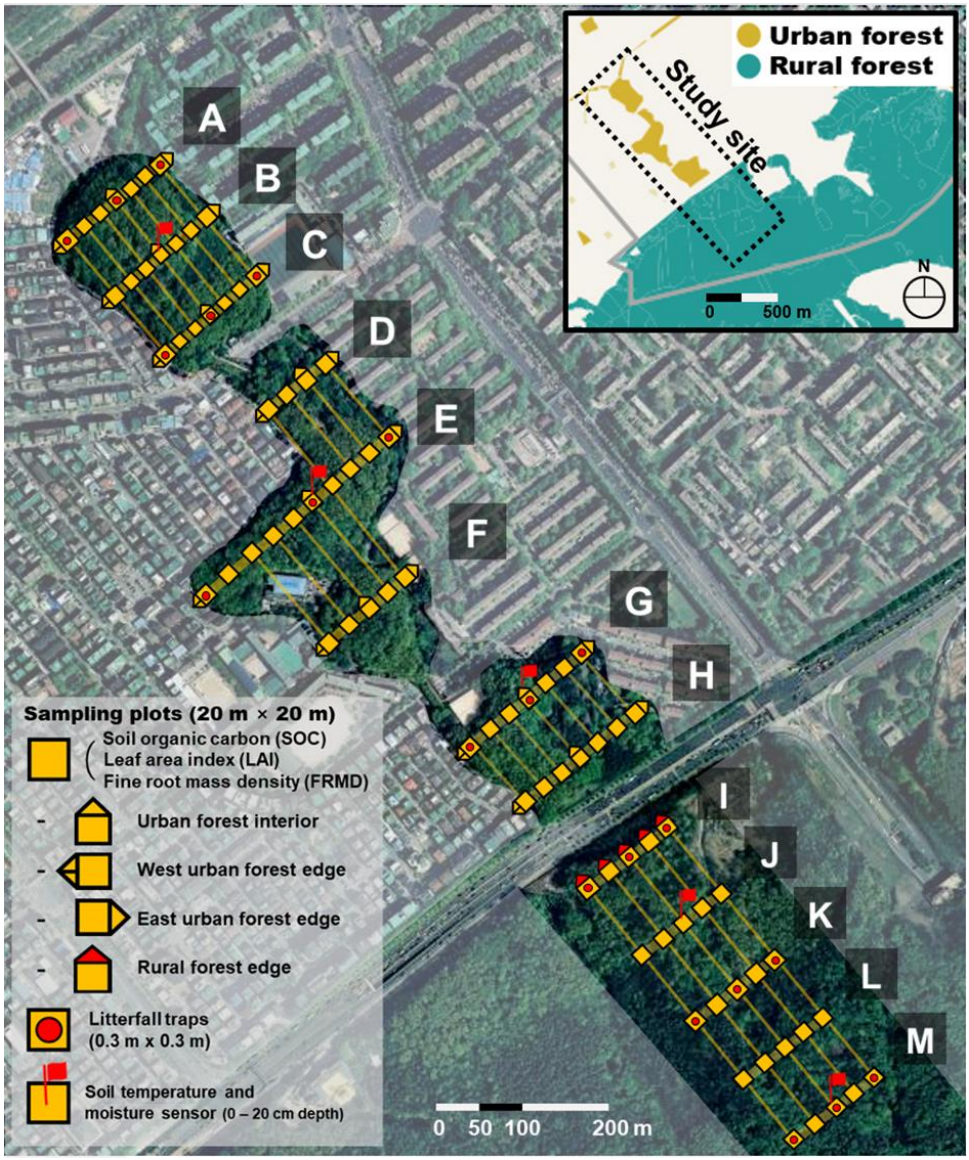

Figure 3.1 Experimental design and setting using two-way transects. The soil survey consisted of urban-rural transects (north to south) crossing urban and rural forests (100 m intervals) and perpendicular transects (west to east) parallel to each other (20 m intervals). Yellow square means the 20 × 20 m plots where SOC, LAI and FRMD data were collected. Urban forest interior, west urban forest edge, east urban forest edge and rural forest edge are marked with three directions of colored triangles, respectively. Locations of

automatic soil temperature and moisture data loggers (red flags), and litterfall traps points (red circles) are marked. Dominant plant species and topographical conditions across transects (A–M) are shown in Table 3.1.

This study was conducted on three fragmented urban forests and a rural forest in Gangnam (Fig. 3.1), Seoul, Republic of Korea. The study site has temperate monsoon climates with hot, humid summers and cold winters. The average annual air temperature is 11.8℃, and the mean annual rainfall is 137.5 cm (Korean Meteorological Administration). The altitude of the area varies between 30 and 60 m within urban forests (transects A–H) and between 50 and 140 m in the rural forest (transects I–M), respectively (Google Earth ver. 7.1.2.2041). The soil parent material is the Gyeonggi gneiss complex consisting of banded gneiss dating to the Precambrian period. According to the Soil and Environmental Information System of Korea (http://soil.rda.go.kr), soils in the urban and rural forests are classified as Inceptisols and Entisols, respectively.

Figure 3.2 Representative view of the urban forest edges. (a) The west edge of the urban forest is adjacent to a paved road. (b) The east forest edge is partially connected to nearby residential greenspace.

The original rural forest was interested by the urban development in the early 1980s, resulting in the three fragmented urban forests (Fig. 3.1). In the urban forest, over the past 40 years, the surrounding land use (i.e., buildings, roads, parking lots) at the

west edge resulted in impervious (paved) surface, whereas the soil surface at the east edge was unpaved and thicker because it is connected to an urban greenspace in residential area (Fig. 3.2). In order to keep the west edge roads clean, litterfall and fallen branch on the west roads were moved to parts of the east forest edge every year (Fig. 3.2b) (personal communication with the park manager). Table 3.1 shows the topographical conditions, total number of soil samples, dominant plant species, and adjacent land use of the study sites.

Table 3.1 Description of sample plots, number of soil samples, mean elevation (m), mean slope angle (°), dominant plant species, and adjacent land use within two different forest types.

Forest type	Transects	*n*	Elevation (m)	Slope angle (°)	Dominant plant species	Adjacent land use (○: greenspace, ●: impervious)			
						East	West	South	North
Urban forests	A	42	29	15	*Betula platyphylla* *Betula davurica* *Pinus rigida* *Prunus sargentii* *Robinia pseudoacacia*	○	●	○	●
	B	42	31	14		○	●	○	○
	C	42	33	14		○	●	●	○
	D	24	28	8		○	●	○	○
	E	60	32	11		○	●	○	●
	F	30	38	15		○	●	○	○
	G	42	51	17		○	●	○	○
	H	42	50	11		○	●	●	○
Rural forest	I	30	70	6	*Betula platyphylla* *Betula davurica* *Quercus mongolica*	○	○	○	●
	J	30	80	18		○	○	○	○
	K	30	101	23	*Pinus koraiensis*	○	○	○	○
	L	30	140	43	*Pinus rigida*	○	○	○	○
	M	30	191	39	*Betula platyphylla* *Quercus mongolica*	○	○	○	○

2.2. Data collection

Soil samples (n = 474) were collected in 79 sampling plots (20 m × 20 m) along two-way transects described above (Fig. 3.1) in June 2017 and July 2018. To quantify the spatial variations of SOC stocks along an urban-rural gradient, we used the 100 m transect crossing urban and rural forests (Fig. 3.1). We defined forest edges as sampling plots (20 m × 20 m) within 20 m distances from the adjacent land use (detailed location is described in Fig. 3.1) because the greatest changes

of abiotic edge effects in the same city tend to occur within this distance (Li et al., 2018). We defined urban forest interiors as core areas in each urban transect (transect A – H). In each sampling plot, six soil samples at 0–20 cm depth were randomly collected using a soil corer (Soil Sampler; Shinill Science, Seoul, Korea) with a 50 mm inner diameter, 51 mm length, and 100 cm^3 volume. To minimize the multi-edge effects within urban forests, urban forest edges with two or more edges within a 20 m distance were not considered from the experimental design.

To identify biotic edge effects, we measured three factors; fine root mass density (FRMD), leaf area index (LAI), and litterfall mass (Lf). To quantify FRMD (g cm^{-3}), we collected fine root samples from the same core as the soil samples in both years. LAI was measured with a LAI-2200 plant canopy analyzer (LI-COR Lincoln, NE, USA). Light scattering correction was performed before the measurement (Kobayashi et al. 2013). A minimum of 12 points were collected randomly in each soil sampling plot (20 m × 20 m). A 90° opening lens cap was used to remove the observer effect of the measurements. Two wands in LAI-2200 were used; one for reference measurements (rooftop of surrounding building, 20 m height) and the other for under canopy measurements. When reading the under-canopy points, the LAI-2200 wand was located 1.3 m above the soil surfaces. Finally, we used the FV2200 software (version 2.1.1; LI-COR Inc.) to compute LAI that considers foliar clumping effects (Ryu et al., 2010). Annual Lf (g m^{-2} yr^{-1}) was collected every month from March to November in litter traps (0.3 m × 0.3 m). Twenty-one litter traps were placed randomly, one for each soil sampling plot (red circles in Fig. 3.1) at a height of 50 cm aboveground. The traps were made of nylon-mesh that allowed throughfall to percolate easily but retained litter particles. To quantify the biomass loss within urban forests, we measured annual pruning yields and litterfall loss from October to February (2017–2019) using litter bags in collaboration with the Department of Urban Park Management.

To identify whether abiotic factors significantly varied near forest edges, we collected soil temperature (Ts) and soil

moisture (volumetric water content [VWC]) data manually and automatically. Continuous Ts and VWC measurement data (GP1 and SM300; Delta-T Devices, Cambridge, UK) were collected at a depth of 20 cm at five plots (red flags in Fig. 3.1) during the growing season (June-August). To measure the spatial patterns of Ts and VWC during the growing season, Ts and VWC data were obtained in all plots weekly from 09:00 to 12:00 (local time) using a portable soil thermometer (MIC99300; Meter Industrial Company, Taichung, Taiwan) and a portable Hydro Sense II with CS658 (20 cm rod) probes (Campbell Scientific, Logan, UT, USA). We manually measured Ts and VWC at a depth of 20 cm, which were cross-calibrated against the continuous measurements.

To investigate the spatial patterns of biotic factors across urban and rural forests, we used normalized difference vegetation index (NDVI) and leaf area index (LAI) from Sentinel-2 from Copernicus Open Access Hub (COAH) during the growing season (day of the year [DOY]; 153 in 2017-2018 and 173 in 2019). The NDVI and LAI were calculated using the Sentinel Application Platform (SNAP), which provides thematic land processing tools for creating visualizations of spectral reflectance. Each of the downloaded scenes was resampled to a spatial resolution of 10 m for each band. The bands of coarser resolution were downscaled using a nearest neighbor algorithm in SNAP.

2.3. Data processing

The soil samples were oven-dried (C-DH; Chang Shin Scientific, Pusan, Korea) at 105℃ for 2 days in the laboratory (USDA-NRCS, 1992). The soil samples were strained through a 2 mm standard testing sieve (Chung Gye Sang Gong, Seoul, Korea) to remove stones. To measure FRMD, we separated dead roots from living roots with tweezers, washed the fine roots (< 2 mm diameter) from the soils, and oven-dried the roots at 70℃ for 2 days (Olsthoorn, 1991). The soil bulk density was determined using the following equation (Adams,

1973):

$$\text{Soil bulk density} = \frac{(\text{total dry mass} - \text{rock mass})}{(\text{total volume} - \text{rock volume}} \quad (1)$$

To estimate the rock volume from the rock mass, we used a standard rock particle density, 2.65 Mg m^{-3} (Brady & Weil, 2007). To remove any inorganic carbon within the soil sample (Edmondson et al., 2015), 10 mL HCI (5.7 M) was added to 2.5 g of each soil sample and the soil samples dried at 105℃ for 24 h. SOC concentration was quantified using an Elemental Analyzer (Flash EA 1112; Thermo Electron, Waltham, MA, USA) at the National Instrumentation Center for Environmental Management (NICEM), Seoul National University. The SOC stocks of unit area (kg m^{-2}) was calculated with the following equation:

$$\text{SOC stock} = [\text{SOC}] \times BD \times d \times 10 \quad (2)$$

where [SOC] is the concentration of SOC in a given soil mass (g kg^{-1}), BD is the bulk density, the soil mass per sample volume (Mg m^{-3}) (Eq. 1), and d is the sampling thickness (m).

2.4. Statistical analyses

All statistical analyses were performed using SigmaPlot 12.0 (Systat Software, Chicago, IL, USA). Analysis of variance (ANOVA) was used, followed by Dunn's test, to test differences in biotic factors (NDVI and LAI), abiotic factors (monthly Ts and VWC), and SOC stocks by proximity to the forest edge. One-way ANOVA with Tukey HSD multiple comparison test was used to analyze differences in annual Lf (g m^{-2} yr^{-1}) between the edges and interiors across urban-rural gradient. We also used the Student's t-test to compare all of the biotic factors in each plot between urban and rural forests. All data are presented as the mean ± 95% confidence interval [CI], unless otherwise specified.

3. Results

3.1. Soil organic carbon (SOC) stocks along an urban–rural gradient

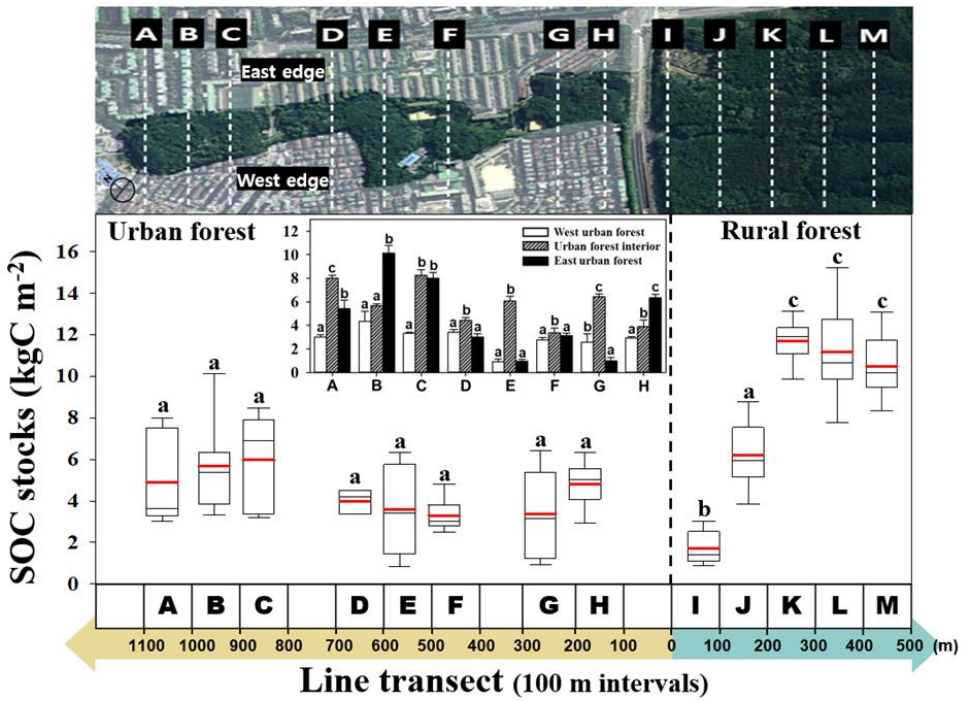

Figure 3.3 SOC stocks (0–20 cm) along an urban–rural gradient from three fragmented urban forests to a large patch of rural forest. The box boundaries represent the 1st and 3rd quartiles, and the black horizontal lines within boxes represent the median value. The lower and upper whiskers represent the 5th and 95th percentiles of the SOC stocks; the red bold line inside the rectangle shows the mean values in each transect. Different letters indicate the significant difference across the transects (Dunn's test, $P < 0.05$). Inset graph shows spatial variations of SOC stocks between the edges and interiors in each urban transect. Different letters in inset graph indicate the significant difference of SOC stocks in each urban transect (Dunn's test, $P < 0.05$). Error bars indicate 95% CI.

Along an urban–rural gradient, the mean SOC stocks (kgC m^{-2}) within the rural forest decreased with proximity to the edge, whereas SOC stocks within urban forests (transects A–H) was not gradually decreases (Dunn's test, $P > 0.05$) (Fig. 3.3). The spatial variations of SOC stocks within urban forests were heterogeneous (Inset in Fig. 3.3). The differences of SOC stocks between the edges and interiors in urban forests (transects A–H) did not show clear patterns. In urban transect A, D, E, F and G, the SOC stocks in the urban forest interiors

was significantly higher than that in the urban forest edges (Inset in Fig. 3.3). The mean SOC stocks in the east edges (B, C and H), however, was similar to or higher than the those for urban forest interiors. In transect B, for instance, a high SOC value (10.58 kgC m^{-2}, a two-fold of mean value) appeared at the east edge. In the rural forest, the SOC stock within the first 20 m of the edges (1.86 kgC m^{-2}) was 80% lower than the forest interiors (10.47 kgC m^{-2}). Although the lowest SOC stocks are found at the edges of rural forest, the rural forest (8.25 kgC m^{-2}) stored on average 1.8 times more SOC stocks than urban forests (4.47 kgC m^{-2}).

3.2. The spatiotemporal variation of abiotic factors across urban and rural forests

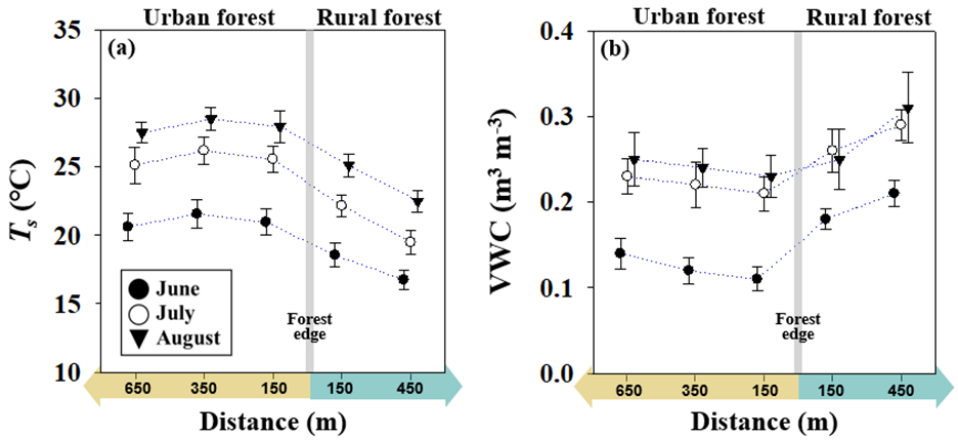

Figure 3.4 Monthly variation in mean soil temperature (*Ts*) and volumetric water content (VWC) at a depth of 20 cm along an urban-rural gradient from urban forest to rural forest. Both *Ts* (℃) and VWC (m^3 m^{-3}) were measured continuously in forest interiors (center plot within each perpendicular transect) during the growing seasons (June to August) in 2017-2018. Error bars indicate 95% CI.

In the rural forest, monthly mean TS consistently increased with proximity to the edge (Dunn's test, $P < 0.05$) during the summer growing seasons (Fig. 3.4a). The monthly mean VWC decreased with proximity to the edge only in June (Fig. 3.4b), when the monthly precipitation (< 120 mm $month^{-1}$) was half that of the other growing seasons (Seoul Station, Korean Meteorological Administration). There was no difference in monthly mean TS or VWC between the urban forest interiors.

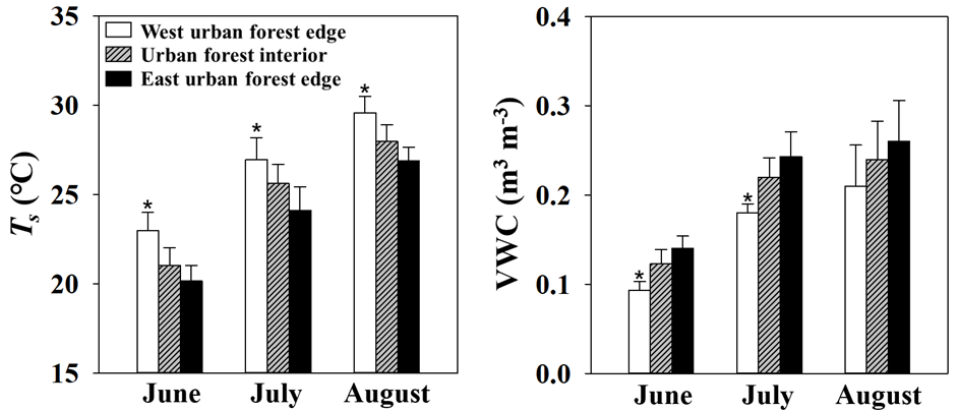

Figure 3.5 Monthly differences in mean soil temperature (T_S) and volumetric water content (VWC) at a depth of 20 cm within urban forests. Both T_S (℃) and VWC (m^3 m^{-3}) were measured continuously in urban forest interiors and manually at each urban forest edge during the growing seasons (June to August) in 2017–2018. Asterisks indicate statistically significant differences of T_S and VWC (Dunn's test, $P < 0.05$). Error bars indicate 95% CI.

We found significant differences in monthly T_S and VWC between the two urban forest edges (west and east) (Fig. 3.5). We found significant summertime differences of T_S (> 2.8℃) and VWC (> 0.05 m^3 m^{-3}) between the two urban forest edges. Monthly mean T_S in the west urban forest edge was significantly higher than in the east urban forest edge (Dunn's test, $P < 0.05$). Except for August, monthly VWC in the west urban forest edge was lower than in the east urban forest edge (Dunn's test, $P < 0.05$).

Table 3.2 Relationship between mean SOC stocks (kgC m^{-2}) and topographic parameters (elevation and slope angle) based on 2017–2018 data from urban and rural forests. The transects are shown in Figure 1.

Forest type	Parameter (units)	Regression model	Adj. R^2	*P*-value
Urban forest	Elevation (m)	Linear regression	0.14	<0.01
(Transects A–H)	Slope angle (°)	Quadratic regression	0.13	<0.01
Rural forest	Elevation (m)	Linear regression	0.49	<0.01
(Transects I–M)	Slope angle (°)	Quadratic regression	0.69	<0.01

Table 3.2 shows the relationships between SOC stocks and topographic parameters, including elevation and slope angle. There is little correlation between SOC stocks and topographic parameters within urban forests (R^2 < 0.14). The spatial distribution of SOC stocks was moderately positively correlated with elevation and slope angle in the rural forest (R^2 > 0.49).

3.3. Relationships between spatial variation of biotic factors and soil organic carbon stocks

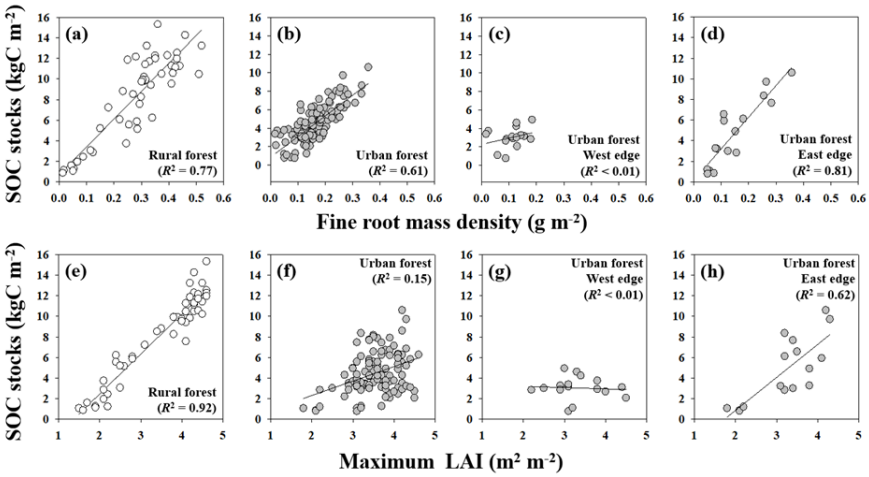

Figure 3.6 Relationship between SOC stocks (kgC m^{-2}) and ground-based biotic factors; fine root mass density and maximum leaf area index (2017-2018). Maximum LAI was defined as peak annual value in each sampling plot (using LAI-2200 plant canopy analyzer). The data in Figure 6b and 6f cover the entire urban forest area, including the urban forest interior, the west urban forest edge and the east urban forest edge. The solid lines represent linear regressions between SOC stocks and biotic factors.

We found significant linear relationships between SOC stocks and FRMD in both rural (R^2 = 0.77) and urban (R^2 = 0.61) forests (Fig. 3.6). In the rural forest, the range of FRMD was 0.02–0.52 g m^{-2}, whereas the range of FRMD in urban forests was 0.01–0.36 g m^{-2}. The relationships between SOC stocks and LAImax varied within and between urban and rural forests (Fig. 3.6b). The mean FRMD and LAImax in urban forest edges were lower than the urban forest interior, but high values were found at the east urban forest edge (Fig. 3.6d and h). In this study, the range in LAImax across all plots based on the data from 2017 and 2018 was 1.5–4.6 m^2 m^{-2}. We found a

significant positive linear correlation between SOC stocks and LAImax in rural forest (R^2 = 0.92) (Fig. 3.6e). Although the correlation between SOC stocks and LAImax of the urban forests was not significant (R^2 = 0.15), the correlation between SOC stocks and LAImax in the east urban forest edges (R^2 = 0.62) was higher than the west urban forest edges (Fig. 3.6b).

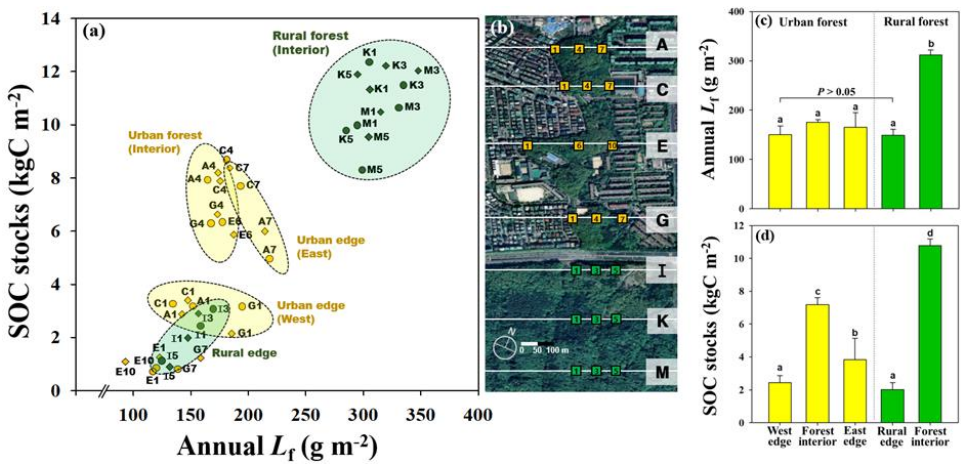

Figure 3.7 Annual litterfall mass (L_f) and SOC stocks along an urban–rural gradient. The spatial distribution of L_f with SOC stocks based on the data from 2017 and 2018 (a), and detail location of litterfall traps in study sites (b). The dashed circles represent broad categories as edge–specific relationship between SOC stocks and L_f across the study sites. Statistical differences in annual L_f (c) and SOC stocks (d) between the edges and interiors (ANOVA, followed by Tukey's test). Error bars indicate 95% CI.

Annual Lf and mean SOC stocks in the rural forest edge (transect I) were significantly lower than its interiors (Fig. 3.7c and d). The range of annual Lf in the rural forest edge was 125–171 g m^{-2}, whereas the range of annual Lf from the other rural forest (transects K–M) was 295–348 g m^{-2}. In the rural forest from the edge to the interior (transects I–M), the spatial distribution of SOC stocks was explained with annual Lf (R^2 = 0.94). In urban forest, there were no significant differences in annual Lf between the forest interior and its edge (Tukey's test, P > 0.05) (Fig. 3.7c); however, the mean values of SOC stocks in west urban forest edges were significantly lower than the other urban forest area (Fig. 3.7d).

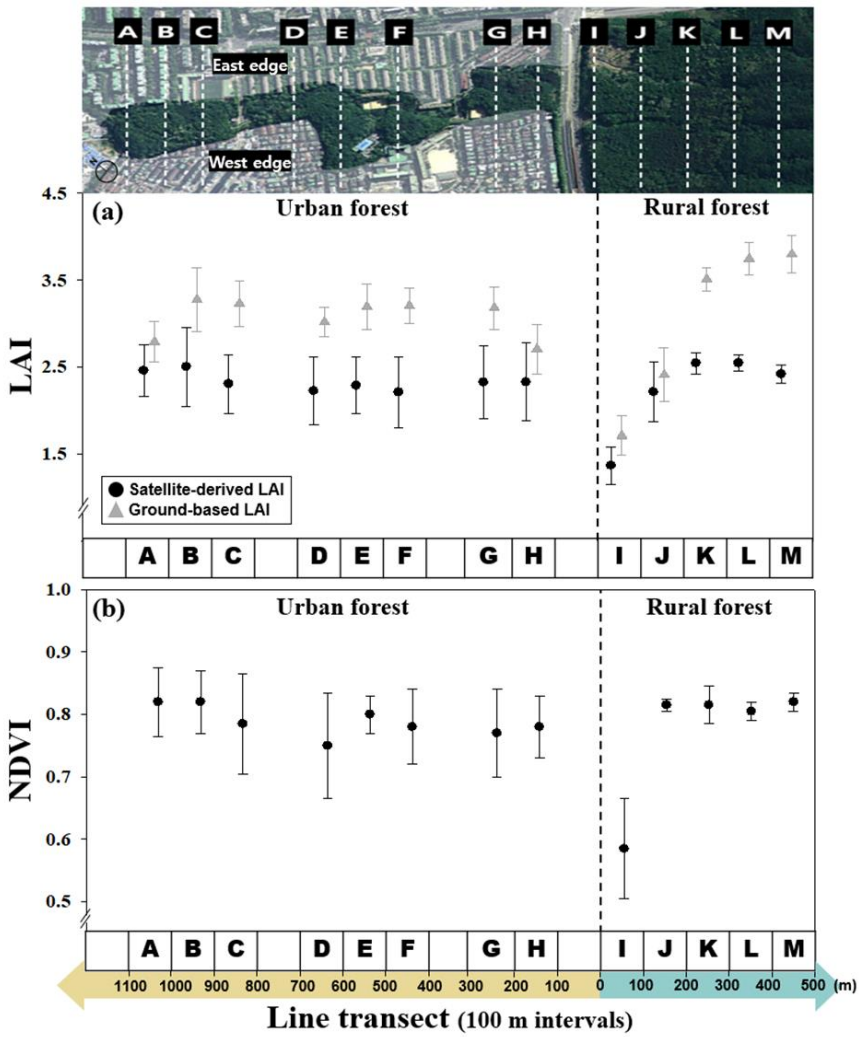

Figure 3.8 The spatial variation of the mean leaf area index (LAI) and the mean normalized difference vegetation index (NDVI) along an urban–rural gradient from urban to rural forests. The LAI and NDVI are derived from Copernicus Sentinel-2 satellite data (June 2, 2017–2018). Light gray symbols in Figure 7a indicate the ground-based LAI using the LAI-2200 instrument (the first week of June, 2017–2018). Error bars indicate 95% CI.

The lowest satellite-derived LAI, NDVI and ground-based LAI values were found at the rural forest edge (transect I) (Dunn's test, $P < 0.05$). Figure 8a shows that the ground-based LAI values in rural forest interiors (transects L–M) were significantly higher than in the overall urban forest area (Dunn's test, $P < 0.05$), whereas satellite-derived LAI and NDVI values were not significantly different between

urban and rural forests (Dunn's test, $P > 0.05$), except in the rural forest edge.

4. Discussion

4.1. Magnitude and causes of edge effects on SOC stocks across urban and rural forests

Our results indicate that above- and belowground biotic factors underpin the rapid decline in SOC stocks at the rural forest edge. Based on satellite and field measurements of canopy structure, the spatial distribution of biotic factors explained the spatial variation in SOC stocks along an urban-rural gradient. The SOC stocks within 20 m of the rural forest edge (1.86 kgC m^{-2}) were 80% lower on average than in the interior (10.47 kgC m^{-2}), and the lowest values for biotic factors (i.e., satellite-derived LAI, NDVI and ground-based LAI) were found in the rural forest edge (Fig. 3.8). The significant decline in both LAI and NDVI in the rural forest edge reported here accords with the results for a study conducted in rural forest edges within 30 m distances from the adjacent roads in the same city (Sung et al., 2018). Figure 6 shows that FRMD accounted for the spatial variation in SOC stocks across urban ($R^2 = 0.61$) and rural ($R^2 = 0.77$) forests, possibly because fine root biomass is the main input source of SOC (Jackson et al., 1997; Bashkin & Binkley, 1998).

Meanwhile, the spatial variation in SOC stocks in the rural forest was affected by topographic parameters ($R^2 > 0.49$) (Table 3.2). Studies reported that topographic conditions such as elevation and slope angle affect the soil moisture variability and carbon dynamics (Bellingrath-Kimura et al., 2015; Zhang et al., 2015). There were no significant correlations between topographic parameters (i.e., slope angle and elevation) and SOC stocks within urban forests (Table 3.2). This could be due to the small differences in topographical conditions within urban forests (Table 3.1).

In urban forests, spatial variation in SOC stocks was likely due to local-scale heterogeneity of abiotic and biotic factors. The mean SOC stocks at the east urban forest edges (4.74 kgC m^{-2}) were 63% greater than at the west urban forest edges (2.9 kgC m^{-2}) (Inset in Fig. 3.3). The higher FRMD influenced SOC stocks at the east urban forest edges (Fig. 3.6d). We found significant differences in monthly

TS and VWC between the two urban forest edges (Fig. 3.5). During the summer growing season, T_S in the west urban forest edges was 2.8℃ higher on average than at the east urban forest edges. The lowest SOC stocks were located in the west urban forest edge (y−axis in Fig. 3.7a), where the soils were generally warmer and drier than inner urban forest soils (Fig. 3.5). By contrast, some soils in the east urban forest edge (transect B) had the highest SOC stocks (10.58 kgC m^{-2}) within urban forests, on par with, or higher than forest interiors in both urban and rural forests (Fig. 3.3).

There was no significant difference in the annual Lf between the urban forest interior and its edge (Fig. 3.7c); however, the SOC stocks at the west urban forest edges were significantly lower than in the other urban forest area (Fig. 3.7d). Figure 3.6 shows the heterogeneity of LAImax within urban forests, and the correlation between LAImax and SOC stocks differs between the west ($R^2 < 0.01$) and east ($R^2 = 0.62$) forest edges. Carbon accumulation in urban soils is explained by the quality and amount of above−ground litter and below−ground root residues (Takahashi et al., 2008; Bae & Ryu, 2015). One explanation for this discrepancy between Lf and SOC stocks at the west urban forest edges is that SOC accumulation was interrupted by repeated disturbances such as litterfall translocation.

4.2. Effects of anthropogenic activities on urban SOC stocks

Our results indicate that human activities at urban forest edges led to contrasting edge effects on SOC stocks (west edge vs. east edge). In this study, most of the litter layer within urban forests was preserved by park managers to support belowground communities, such as earthworm populations. As mentioned in the Methods, however, litterfall in the west urban forest edges flew to the road via the downslopes (Fig. 3.2a), which was artificially translocated to the east urban forest edges. In collaboration with the park management department between 2017 and 2019, we quantified the mean annual pruning yields (2.2 ± 0.3 ton yr^{-1}) and Lf (3.8 ± 0.5 ton yr^{-1}) on the road near the west edges. Surprisingly, the Lf on the road was similar to or higher than the annual Lf within west edges (3.2 ton yr^{-}

[1]), which was calculated by multiplying the total area of the west urban forest edge (within 20 m distance) and the annual Lf derived by litter traps (Fig. 3.7b). Therefore, we assume that the well-preserved litter layers at the east urban forest edges, which received additional Lf from the west edges, led to enhanced SOC stocks.

The SOC accumulation in urban forest edges was constrained by the adjacent land use. Our finding shows that differences in land management (litter removal and litter addition) between urban forest edges contributed to the contrasting edge effects on SOC stocks. This is further exemplified in long-term field experiment, Lajtha et al. (2014) found significant decreases in soil organic matter under litter removals. In this site, the west forest edges were characterized with discrete surfaces from asphalt road to the forest. According to previous urban studies (Delgado et al., 2007; Hamberg et al., 2009), some urban features, such as cutting edges and asphalt roads, cause a highly significant TS gradient (> 9℃) from the forest edge to the forest interior. During the growing seasons, TS in the west urban forest edges was on average 1.6℃ and 2.8℃ higher than in the urban forest interiors and east urban forest edges, respectively (Fig. 3.5), which might be attributed to litterfall translocations to the east edges which led almost absence in litter layers in the west edges. According to Bae & Ryu (2017), in the same city, a summertime difference of TS (> 2.5℃) in an urban forest can boost soil respiration by up to 20% which could reduce SOC accumulation.

We argue that efforts should be made to characterize and quantify human impacts to understand edge effects on SOC stocks. Pruning, trimming, reshaping, and litter removal are common land management practices in urban areas (Singh et al., 2017), and these residues can result in a significant change in SOC stocks in a managed landscape (Jo & McPherson, 1995; Bae & Ryu, 2015). In addition to these repeated human activities, the unpaved surface at the forest edge may act as a buffer zone mitigating abiotic edge effects (Delgado et al., 2007; Crockatt, 2012). A recent research has shown that forest growth rates in urban forest edges nearly double from the interiors because of increases in available solar radiation so leaf area

index (Reinmann et al., 2020). We did not find clear patterns of higher LAI in urban forest edges than interiors in our site (data not shown). Instead, we found that the high values of fine root productivity in east forest edges (e.g. transect B and H in Fig. 3.6d) where litter layer is well-preserved. Our results suggest that the low SOC stocks in west urban forest edges offer a potential for carbon sequestration through improved land management practices. Recent research revealed that 85% of the greenspaces in Boston, Massachusetts are within 10 m of an edge (Trlica et al., 2019). As edges become prominent landscape features in urban regions (Reinmann et al., 2020), quantifying the edge effects on SOC stocks will become increasingly important for making urban carbon policy. We call for more efforts to understand the various mechanisms underlying the edge effect on SOC stocks in fragmented urban landscapes.

5. Conclusion

Our results indicate that the magnitude and cause of edge effects on SOC stocks varied within fragmented landscapes, and that human activities alter SOC stocks in urban landscapes. The declines in above- and belowground biotic factors (i.e., LAI, NDVI, Lf and FRMD) observed in plots located closer to the rural forest edges underpin significant declines in SOC stocks. The differences of urban SOC stocks between the edges and interiors did not show clear patterns; however, the SOC stocks at the east edges (4.74 kgC m^{-2}) were 63% greater than at the west edges (2.9 kgC m^{-2}), and were explained by the adjacent land use and litterfall management practices. The impact of fragmentation on urban SOC stocks is due to more than just the direct effect of biotic factors; it also involves the indirect effects of human activities, which adds complexity compared to the impacts on SOC decline at rural edges. This latter effect is a key mechanism in the observed response to SOC change at urban forest edges. This study provides insight into the relationship between forest fragmentation and SOC stocks, which involves a combination of natural and anthropogenic factors.

Chapter 4: Spatial variations of soil organic carbon under diverse land cover types: application of laboratory-based hyperspectral reflectance spectroscopy

1. Introduction

Urbanization and land use change are accompanied by increasing anthropogenic pressure to soils (Herrmann et al., 2018). Urban soils are heterogeneous mixture of various parent materials and significantly affected by anthropogenic activities (Bae & Ryu, 2020). The natural source of soil organic carbon (SOC) is plant materials (Guo et al., 2007; Ladd et al., 2014), but urban materials provide an additional source of SOC in urban area (Guo et al., 2013). Tracing the source of SOC in diverse land use pattern is important for assessing the consequences of urbanization on SOC budgets. The relationship between SOC change and human activities, however, is primarily focused on agricultural and forest soils.

Understanding the consequences of human activities on SOC is increasingly important with the expanding urban land area (Vasenev & Kuzyakov, 2018). Improving our understanding of the relationships between the pattern of land cover and the SOC requires large amounts of timely and cost efficient SOC analysis, which is difficult to obtain with routine chemical analysis. Evaluation of SOC stocks need to be rapidly scaled up and implemented to contribute to climate change mitigation. To manage SOC budgets at the city scale, there is an urgent need to qualify both SOC stocks and their sources (Guo et al., 2017; Rogers et al., 2017). Stable carbon isotopes are considered as an invaluable tool for monitoring SOC, both as a tracer and as a record of processes in which isotopic fractionation occurs (Bowling et al., 2008). Extensive soil sampling is required at city scale to accurately estimate the SOC and the carbon isotopic composition (expressed as $\delta^{13}C$), however, it is an expensive and time-consuming process. Therefore, a rapid and cost-effective alternative method to quantify SOC and $\delta^{13}C$, with acceptable precision, is needed.

Soil spectroscopy is the "reflectance part of the electromagnetic radiation that interacts with the soil matter across

the visible near-infrared (VIS-NIR) spectral region (Ben-Dor & Banin, 1995). With minimal sample preparation and no use of chemicals, VIS-NIR spectroscopy provides a fast, cost-effective, and relatively accurate alternative method for SOC contents estimation (Stevens et al., 2008). A previous study demonstrated that NIR spectra should be able to capture the differences in the atomic mass of the soil carbon isotope (Kleinebecker et al., 2009). Fuentes et al. (2012) explored the possibility to predict soil $\delta^{13}C$ values using NIR spectra. Using modified partial least squares (MPLS) regression, they developed calibration models with an R^2 of 0.81 (Fuentes et al., 2012).

In this work, we present a case study where we use spectroscopy of soils to develop predictive models for SOC, exploring the application of this approach in the scaling of urban soil analysis to city scale assessments of soil health. Specific objectives of this study include: 1) to quantify the spatial variations of SOC and $\delta^{13}C$ among different land cover; 2) to assess the potential for spectroscopy to predict for SOC under heterogeneous urban land cover types.

2. Materials and Methods

2.1. Site description and Data collection

This study was conducted in the GwaunGyo Lake Park, Suwon, Republic of Korea (37.283118° N, 127.065927° E). The parent material is underlain by Daebo granite from the Quaternary period. According to the Soil and Environmental Information System of Korea (http://soil.rda.go.kr), the soils in the park are classified as Cambisols.

Soil samples were collected from June 2019 and June 2020. A total of 136 topsoil samples (0-20 cm) were collected and the SOC concentration (%) and $\delta^{13}C$ values (‰) were measured under six land cover types, including mixed forests (n=24), broad-leaf forest (n=24), needle-leaf forest (n=24), lawn (n=24), wetland (n=24) and bare land (n=16) in GwaunGyo Lake Park. Land-cover is defined as the physical land type such as vegetation types. The dominant plant species included, *Quercus acutissima*, *Quercus mongolica*, and *Pinus rigida* in mixed forest, *P. rigida* a

nd *Pinus strobus* in needle-leaf forest, *Q. acutissima*, *Q. mongolica*, and *Quercus serrata* in broadleaf forest, *Zoysia japonica* in lawn and *Phragmites japonica*, *Phragmites communis*, and *Miscanthus sacchariflorus* in wetland. Except bare land, we randomly selected eight plots (10 × 10 quadrats) in each vegetation type. At each plot, we removed the litter layer and collected three soil samples using a soil corer (Soil Sampler; Shinill Science Inc., Seoul, Korea) with a 50 mm inner diameter, 51 mm length, and 100 cm^3 volume.

2.1. Data processing

Individual soil samples were oven-dried (C-DH; Chang Shin Scientific, Pusan, Korea) at 105℃ for 48 h in the laboratory (USDA-NRCS 1992). The soil samples were strained through a 2 mm standard testing sieve (Chung Gye Sang Gong, Seoul, Korea) to remove stones. To remove any inorganic carbon within the soil sample (Edmondson et al. 2015), 10 mL HCI (5.7 M) was added to 2.5 g of each soil sample and the soil samples dried at 105℃ for 24 h. SOC concentration (%) was quantified using an Elemental Carbon Analyzer (Flash EA 1112; Thermo Electron, Waltham, MA, USA) at the National Instrumentation Center for Environmental Management (NICEM), Seoul National University.

The isotopic compositions (expressed as ^{13}C) were measured in the topsoil (0–0.2 m). ^{13}C was determined with continuous-flow isotope ratio mass spectrometry (OPTIMA, Micromass, UK Ltd) at the NICEM. Carbon isotope ratio ($\delta^{13}C$) is calculated using the following equation (Farquhar et al., 1989):

$$\delta\,13C = \left\{ \frac{\left(\frac{13C}{12C}\right)sample}{\left(\frac{13C}{12C}\right)standard} - 1 \right\} \times 1000$$

where the standard is the ratio of PDB (Pee Dee Belemnite).

Hyperspectral reflectance for each soil sample was collected using a full range vis-NIR spectrometer (ASD-FieldSpec, Analyt

ical Spectral Devices Inc., Boulder, CO, USA) from 350 to 2500 nm wavelength with a sampling interval of 1 nm. The ASD spectrometer was used in a bare fibre optic configuration with a 25° view angle. All spectra were recorded using a standard contact probe that embeds both an optical fibre and a halogen bulb light. Before spectral acquisition of each soil sample, the ASD spectrometer was optimized on a dark current followed by a white reference panel (Spectralon®). The single spectrum for a given soil sample was an average of 10 scans and the final spectrum used in the treatment was an average of the six replicates.

A partial least squares (PLS) regression to establish the predictive models for SOC concentration in urban soils. PLSR, a classical non-parametric linear regression method, has been widely used in soil spectral analysis (Hbirkou et al., 2012). When reducing the numbers of predictor, PLSR also decreases the risk induced by multicollinearity of predictors (Hu et al., 2017). So, PLSR was suitable choice for analysing soil spectra that contain thousands of wavelengths. To avoid over-fitting or under-fitting, leave-one-out cross validation (LOOCV) was applied to optimize the number of latent variables in the calibration. For the regression model, the predictive power of spectroscopic measurements can be described by the coefficient of determination (R^2) between measured SOC and predicted SOC values. The root-mean-square-error of prediction (RMSE) was used to assess the accuracy of the SOC prediction model. Variable importance in the projection (VIP) was applied to select variables.

2.2. Statistical analyses

Statistical analyses were conducted using SigmaPlot 12.0 software (Systat Software Inc., Chicago, IL, USA). We used one-way analysis of variance (ANOVA) followed by Dunn's multiple comparison test to compare SOC concentration (%) and $\delta^{13}C$ values of topsoil within land cover types. All data are presented as means ± 95% CI unless otherwise specified.

3. Results and discussion

3.1. Spatial variations of SOC concentration and $\delta^{13}C$ among different land cover types

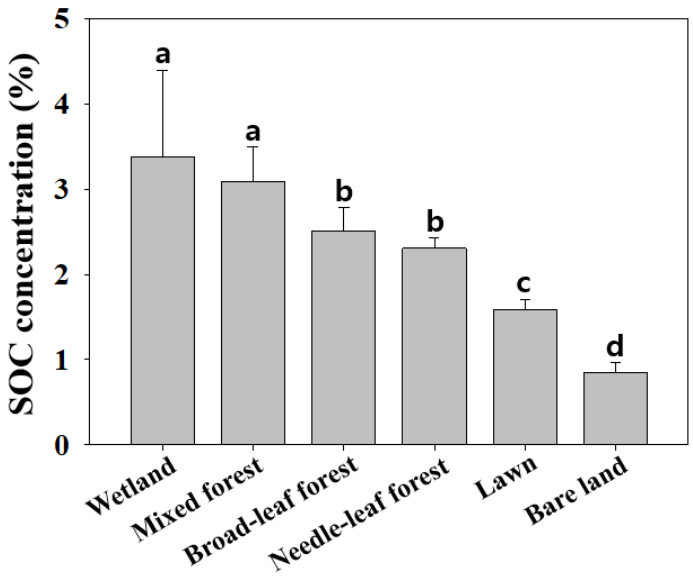

Figure 4.1 Soil organic carbon (SOC) concentration (%) with different land cover types. Different letters indicate the significant difference across the land cover types (Dunn' test, $P < 0.05$). Error bars indicate 95% CI of SOC concentration at a depth of 0.2 m.

Urban parks are characterized by a diverse land cover. In this study, we found that different land cover types lead to spatial heterogeneity of SOC concentration and $\delta^{13}C$ values. A greater than fourfold difference in SOC concentration was observed at topsoil (0–0.2 m) across the six different land cover types (Fig. 4.1). The highest SOC concentration in the topsoil was located in wetland area (3.38 ± 1.02 %). In contrast, the lowest SOC concentration was located in bare land (0.85 ± 0.12 %). We found a twofold difference in SOC concentration between mixed forest soils (3.10 ± 1.02 %) and lawn soils (1.59 ± 0.12 %). Except wetland soils, the SOC concentration in mixed forest (3.10 ± 0.12 %) was significantly higher than those of the other forest types ($P < 0.05$; Fig. 4.1). No significant difference was detected in SOC concentration of broad–leaf forest (2.51 ± 0.27 %) and the needle–leaf forest (2.31 ± 0.12 %) ($P < 0.05$; Fig. 4.1). A previous study in constructed urban

park reported that SOC concentration in mixed forests (2.6 ± 0.3 %) were seven times greater than bare soils (0.35 ± 0.1 %) (Bae & Ryu, 2015). Such variation of SOC among heterogeneous land cover types is common in urban park (Golubiewski, 2006; Edmondson et al., 2012).

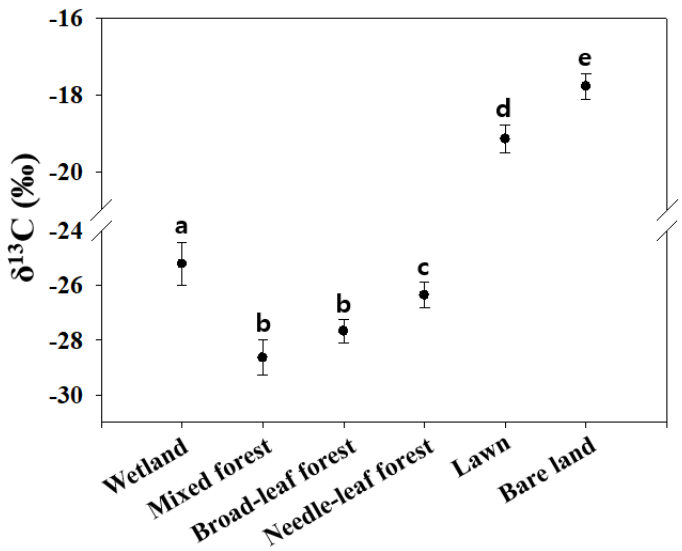

Figure 4.2 Spatial variations of soil $\delta^{13}C$ among different land cover types. Different letters indicate the significant difference across the land cover types (Dunn' test, $P < 0.05$). Error bars indicate 95% CI.

There were significant differences among heterogeneous land cover types in terms of $\delta^{13}C$ in the topsoil (0–0.2 m) (Fig. 4.2). The topsoil $\delta^{13}C$ values in bare land (−17.7 ± 0.3‰) and lawn area (−19.2 ± 0.4‰) were more enriched (less negative) than other land cover types. The $\delta^{13}C$ values in wetland (−25.2 ± 0.8‰) were more enriched (less negative) than those under forests types (mixed forest: −28.6 ± 0.6‰, broad−leaf forest: −27.7 ± 0.4‰, needle−leaf forest: −26.4 ± 0.5‰). We found no significant difference in topsoil $\delta^{13}C$ values between mixed forests and broad−leaf forests (Dunn' test, $P > 0.05$). The heterogeneous soil $\delta^{13}C$ values, in this study, indicates that carbon source in urban park stemmed from both natural and anthropogenic conditions. A previous study in urban landscape reported that soil $\delta^{13}C$ in Karlsruhe to vary between −15.6‰ to −29.3‰ (Norra et al.; 2005). This range is very similar to the range of our study site. The $\delta^{13}C$ values are related to organic carbon derived from plant biomass and addition of carbon containing

urban settings (Boeckx et al., 2006). The most enriched soil $\delta^{13}C$ values ($-17.7 \pm 0.3‰$), in this study, were found in bare land (Fig. 4.2). Previous study reported that concrete materials have $\delta^{13}C$ values from $-8.0‰$ to $-17.5‰$ (Norra et al., 2005; Schleicher et al., 2013), comparable to those in the topsoil in bare land. Meanwhile, the range of soil $\delta^{13}C$ under three types of forests ($-28‰$ to $-26‰$) is consistent with urban forest ($-28‰$ to $-24‰$) in the Asian monsoon climate (Guo et al., 2013; Guo et al., 2017).

3.2. Assessments of urban SOC concentration using reflectance spectroscopy

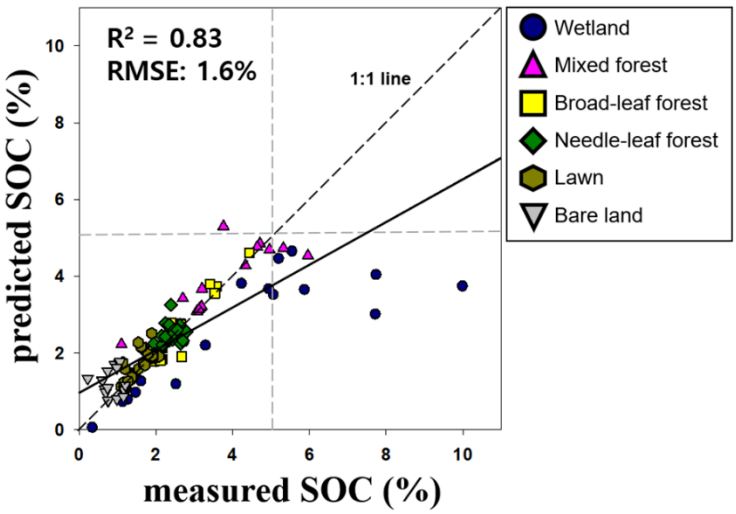

Figure 4.3 Prediction scatter plot of soil organic carbon (SOC) concentration.

The PLSR model achieved acceptable performance with coefficent of determination (R^2) and root mean square error (RMSE) of calibration set for SOC concentration (R^2 = 0.83; RMSE = 1.6%). The leave-one-out cross-validation (LOOCV) procedure confirmed the robust performance of PLSR model. Most of the sample points, in this study, with measured SOC values < 5% had prediction SOC values <5%; for samples with SOC values >5%, the predicted SOC values were generally underestimated (Fig. 4.3). The predicted SOC especially in wetland area have been underestimated. It is possible that species characteristics in wetland may have resulted in different forms and types of SOC such as dissolved organic carbon

(Cohen et al., 2005) whose concentration depends on photosynthetic activity in the wetland ecosystem (Gergel et al., 1999).

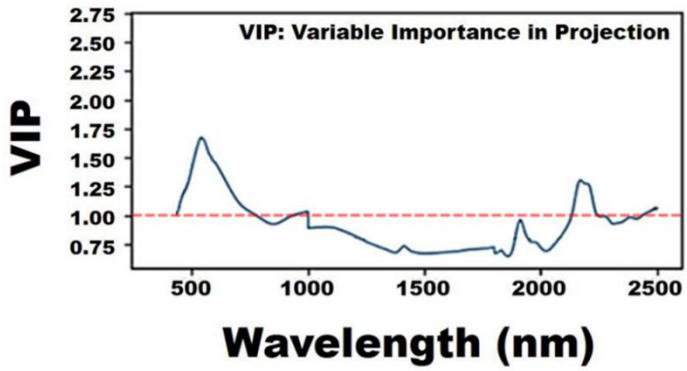

Figure 4.4 Variable Importance in Projection (VIP) scores of optimized PLSR model.

The prediction VIP scores of different spectral bands of the optimized PLSR model were presented in Fig 4.4. According to the VIP scores, urban SOC in oven-dried soil samples can be accurately predicted by mean of visible (VIS, 400-700 nm) and near infrared (NIR, 2200-2300) diffuse reflectance spectroscopy (Fig. 4.4, 1>VIP). The VIS part of the spectrum between 400 and 700 nm had a large influence on calibrations. This range is similar to the typical ranges for SOC prediction (Cozzolino and Morón, 2006). These wavelengths (VIS, 400-700 nm) are thought to be associated with absorption from plant residues (Morra et al., 1991; Salgó et al., 1998). Previous study reported that the wavelength at 2218 nm was previously correlated with SOC in the whole soil (Morra et al., 1991).

4. Conclusions

Efficient low-carbon policy and soil management require detailed information on the spatial distribution of SOC. A major limitation to evaluating urban carbon budgets is the cost of measuring SOC. Soil spectroscopy has great potential to predict SOC in heterogeneous urban landscapes. Our results indicated that the SOC can be estimated with reasonable accuracy across urban vegetated area

based solely on the hyperspectral reflectance spectroscopy, and the strategy has the potential of upscaling for city scale assessments of SOC budgets. We suggest that urban SOC studies could successfully integrate VIS–NIR analysis to fill data gaps in the spatial analysis of SOC. Despite these promising results, caution should be taken regarding the nature of sampling and number of samples analysed for developing prediction equations. Among six land cover types, the accuracy of SOC prediction in wetland was not considered good enough to replace routine chemical analysis methods. Further work is required to resolve the effect of soil type and different form of SOC with large sample size in order to expand the utilization of spectroscopy for SOC prediction in urban ecosystem.

References

Adams, W. A. 1973. Effect of organic matter on bulk and true densities of some uncultivated podzolic soils. Journal of Soil Science 24:10–17.

Bae, J., and Y. Ryu. 2015. Land use and land cover changes explain spatial and temporal variations of the soil organic carbon stocks in a constructed urban park. Landscape and Urban Planning 136:57–67.

Bae, J., and Y. Ryu. 2017. Spatial and temporal variations in soil respiration among different land cover types under wet and dry years in an urban park. Landscape and Urban Planning 167:378–385.

Bae, J., and Y. Ryu. 2020. High soil organic carbon stocks under impervious surfaces contributed by urban deep cultural layers. Landscape and Urban Planning 204:103953.

Barros, H. S., and P. M. Fearnside. 2016. Soil carbon stock changes due to edge effects in central Amazon forest fragments. Forest Ecology and Management 379:30–36.

Bashkin, M. A., and D. Binkley. 1998. Changes in soil carbon following afforestation in Hawaii. Ecology 79:828–833.

Bateman, A. S., and S. D. Kelly. 2007. Fertilizer nitrogen isotope signatures. Isotopes in Environmental and Health Studies 43:237–247.

Bellingrath-Kimura, S. D., A. W. Kishimoto-Mo, N. Oura, S. Sekikawa, S. Yonemura, S. Sudo, A. Hayakawa, K. Minamikawa, Y. Takata, and H. Hara. 2015. Differences in the Spatial Variability Among CO2, CH4, and N2O Gas Fluxes from an Urban Forest Soil in Japan. Ambio 44:55–66.

Ben-Dor, E., and A. Banin. 1995. Near-infrared analysis as a rapid method to simultaneously evaluate several soil properties. Soil Science Society of America Journal 59:364–372.

Bielinska, E. J., B. Kolodziej, and D. Sugier. 2013. Relationship between organic carbon content and the activity of selected enzymes in urban soils under different anthropogenic influence. Journal of

Geochemical Exploration 129:52−56.

Boeckx, P., M. Van Meirvenne, F. Raulo, and O. Van Cleemput. 2006. Spatial patterns of delta C−13 and delta N−15 in the urban topsoil of Gent, Belgium. Organic Geochemistry 37:1383−1393.

Bowling, D. R., D. E. Pataki, and J. T. Randerson. 2008. Carbon isotopes in terrestrial ecosystem pools and CO2 fluxes. New Phytologist 178:24−40.

Brady, N. C., and R. R. Weil. 2007. The Nature and Properties of Soils. Prentice Hall; 14 edition (September 16, 2007), Lebanon, Indiana, U.S.A.

Broere, W. 2016. Urban underground space: Solving the problems of today' s cities. Tunnelling and Underground Space Technology 55:245−248.

Camargo, J., and V. Kapos. 1995. Complex edge effects on soil moisture and microclimate in central Amazonian forest. Journal of Tropical Ecology 11:205−221.

Chaopricha, N. T., and E. Marin−Spiotta. 2014. Soil burial contributes to deep soil organic carbon storage. Soil Biology & Biochemistry 69:251−264.

Churkina, G. 2008. Modeling the carbon cycle of urban systems. Ecological Modelling 216:107−113.

Cohen, M. J., Prenger, J. P., & DeBusk, W. F. (2005). Visible-near infrared reflectance spectroscopy for rapid, nondestructive assessment of wetland soil quality.Journal of environmental quality,34(4), 1422−1434.

Cozzolino, D., and A. Morón. 2006. Potential of near−infrared reflectance spectroscopy and chemometrics to predict soil organic carbon fractions. Soil and Tillage Research 85:78−85.

Crockatt, M. E. 2012. Are there edge effects on forest fungi and if so do they matter? Fungal Biology Reviews 26:94−101.

Delgado, J. D., N. L. Arroyo, J. R. Arévalo, and J. M. Fernández−Palacios. 2007. Edge effects of roads on temperature, light, canopy cover, and canopy height in laurel and pine forests (Tenerife, Canary

Islands). Landscape and Urban Planning 81:328−340.

Edmondson, J. L., Z. G. Davies, N. McHugh, K. J. Gaston, and J. R. Leake. 2012. Organic carbon hidden in urban ecosystems. Scientific Reports 2:963.

Edmondson, J. L., I. Stott, J. Potter, E. Lopez−Capel, D. A. Manning, K. J. Gaston, and J. R. Leake. 2015. Black carbon contribution to organic carbon stocks in urban soil. Environmental science & technology 49:8339−8346.

Elvidge, C. D., B. T. Tuttle, P. S. Sutton, K. E. Baugh, A. T. Howard, C. Milesi, B. L. Bhaduri, and R. Nemani. 2007. Global distribution and density of constructed impervious surfaces. Sensors 7:1962−1979.

Fang, Y., M. Yoh, K. Koba, W. Zhu, Y. Takebayashi, Y. Xiao, C. Lei, J. Mo, W. Zhang, and X. Lu. 2011. Nitrogen deposition and forest nitrogen cycling along an urban–rural transect in southern China. Global Change Biology 17:872−885.

Farquhar, G. D., J. R. Ehleringer, and K. T. Hubick. 1989. Carbon isotope discrimination and photosynthesis. Annual Review of Plant Physiology and Plant Molecular Biology 40:503−537.

Fuentes, M., C. Hidalgo, I. González−Martín, J. Hernández−Hierro, B. Govaerts, K. Sayre, and J. Etchevers. 2012. NIR spectroscopy: an alternative for soil analysis. Communications in Soil Science and Plant Analysis 43:346−356.

Gee, G. W., and J. W. Bauder. 1979. Particle size analysis by hydrometer − simplified method for routine textural analysis and a sensitivity test of measurement parameters. Soil Science Society of America Journal 43:1004−1007.

Gehlhausen, S. M., M. W. Schwartz, and C. K. Augspurger. 2000. Vegetation and microclimatic edge effects in two mixed−mesophytic forest fragments. Plant Ecology 147:21−35.

Gergel, S. E., M. G. Turner, and T. K. Kratz. 1999. Dissolved organic carbon as an indicator of the scale of watershed influence on lakes and rivers. Ecological Applications 9:1377−1390.

Golubiewski, N. E. 2006. Urbanization increases grassland carbon pools: Effects of landscaping in Colorado's front range. Ecological Applications 16:555−571.

Gong, C., S. Yu, H. Joesting, and J. Chen. 2013. Determining socioeconomic drivers of urban forest fragmentation with historical remote sensing images. Landscape and Urban Planning 117:57−65.

Guo, L. B., M. Wang, and R. M. Gifford. 2007. The change of soil carbon stocks and fine root dynamics after land use change from a native pasture to a pine plantation. Plant and Soil 299:251−262.

Guo, Q. J., H. Strauss, T. B. Chen, G. X. Zhu, J. Yang, J. X. Yang, M. Lei, X. Y. Zhou, M. Peters, Y. F. Xie, H. Z. Zhang, R. F. Wei, and C. Y. Wang. 2013. Tracing the source of Beijing soil organic carbon: A carbon isotope approach. Environmental Pollution 176:208−214.

Guo, Q. J., G. X. Zhu, T. B. Chen, J. Yang, J. X. Yang, M. Peters, R. F. Wei, L. Y. Tian, X. K. Han, and J. Hu. 2017. Spatial variation and environmental assessment of soil organic carbon isotopes for tracing sources in a typical contaminated site. Journal of Geochemical Exploration 175:11−17.

Haddad, N. M., L. A. Brudvig, J. Clobert, K. F. Davies, A. Gonzalez, R. D. Holt, T. E. Lovejoy, J. O. Sexton, M. P. Austin, and C. D. Collins. 2015. Habitat fragmentation and its lasting impact on Earth’s ecosystems. Science Advances 1:e1500052.

Hamberg, L., S. Lehvävirta, and D. J. Kotze. 2009. Forest edge structure as a shaping factor of understorey vegetation in urban forests in Finland. Forest Ecology and Management 257:712−722.

Harris, L. D. 1988. Edge effects and conservation of biotic diversity. Conservation Biology 2:330−332.

Hara, Y., K. Takeuchi, and S. Okubo. 2005. Urbanization linked with past agricultural landuse patterns in the urban fringe of a deltaic Asian mega−city: a case study in Bangkok. Landscape and Urban Planning 73:16−28.

Hbirkou, C., S. Pätzold, A.−K. Mahlein, and G. Welp. 2012. Airborne hyperspectral imaging of spatial soil organic carbon

heterogeneity at the field-scale. Geoderma 175:21-28.

Herrmann, D. L., L. A. Schifman, and W. D. Shuster. 2018. Widespread loss of intermediate soil horizons in urban landscapes. Proceedings of the National Academy of Sciences of the United States of America 115:6751-6755.

Hu, B., S. Chen, J. Hu, F. Xia, J. Xu, Y. Li, and Z. Shi. 2017. Application of portable XRF and VNIR sensors for rapid assessment of soil heavy metal pollution. PloS one 12:e0172438.

Jackson, R. B., H. Mooney, and E.-D. Schulze. 1997. A global budget for fine root biomass, surface area, and nutrient contents. Proceedings of the National Academy of Sciences 94:7362-7366.

Jo, H. K., and E. G. McPherson. 1995. Carbon storage and flux in urban residential greenspace. Journal of Environmental Management 45:109-133.

Keiluweit, M., T. Wanzek, M. Kleber, P. Nico, and S. Fendorf. 2017. Anaerobic microsites have an unaccounted role in soil carbon stabilization. Nature communications 8:1771.

Kim, D.-S., K. Mizuno, and S. Kobayashi. 2003. Analysis of urbanization characteristics causing farmland loss in a rapid growth area using GIS and RS. Paddy and Water Environment 1:189-199.

Kleinebecker, T., S. R. Schmidt, C. Fritz, A. J. Smolders, and N. Hölzel. 2009. Prediction of $\delta^{13}C$ and $\delta^{15}N$ in plant tissues with near-infrared reflectance spectroscopy. New Phytologist 184:732-739.

Kobayashi, H., Y. Ryu, D. D. Baldocchi, J. M. Welles, and J. M. Norman. 2013. On the correct estimation of gap fraction: How to remove scattered radiation in gap fraction measurements? Agricultural and Forest Meteorology 174:170-183.

Krauss, J., R. Bommarco, M. Guardiola, R. K. Heikkinen, A. Helm, M. Kuussaari, R. Lindborg, E. ckinger, M. Pärtel, and J. Pino. 2010. Habitat fragmentation causes immediate and time-delayed biodiversity loss at different trophic levels. Ecology letters 13:597-605.

Kuang, W. H., L. J. Chen, J. Y. Liu, W. N. Xiang, W. F. Chi, D. S.

Lu, T. R. Yang, T. Pan, and A. L. Liu. 2016. Remote sensing-based artificial surface cover classification in Asia and spatial pattern analysis. Science China-Earth Sciences 59:1720-1737.

Kvenvolden, K. A., P. R. Carlson, A. Warden, and C. N. Threlkeld. 1998. Carbon isotopic comparisons of oil products used in the developmental history of Alaska. Chemical Geology 152:73-84.

Lajtha, K., K. L. Townsend, M. G. Kramer, C. Swanston, R. D. Bowden, and K. Nadelhoffer. 2014. Changes to particulate versus mineral-associated soil carbon after 50 years of litter manipulation in forest and prairie experimental ecosystems. Biogeochemistry 119:341-360.

Ladd, B., P. L. Peri, D. A. Pepper, L. C. R. Silva, D. Sheil, S. P. Bonser, S. W. Laffan, W. Amelung, A. Ekblad, P. Eliasson, H. Bahamonde, S. Duarte-Guardia, and M. Bird. 2014. Carbon isotopic signatures of soil organic matter correlate with leaf area index across woody biomes. Journal of Ecology 102:1606-1611.

Lee, K.-S., and W.-J. Kim. 2009. The development and use of fertilizer for 40 years in Korea. Korean Journal of Soil Science and Fertilizer 42:195-211.

Lee, S., Y. Ryu, and C. Jiang. 2015. Urban heat mitigation by roof surface materials during the East Asian summer monsoon. Environmental Research Letters 10(12):124012.

Li, C., L. Zhao, P. Sun, F. Zhao, D. Kang, G. Yang, X. Han, Y. Feng, and G. Ren. 2016. Deep Soil C, N, and P Stocks and Stoichiometry in Response to Land Use Patterns in the Loess Hilly Region of China. PloS one 11:e0159075.

Li, Y., W. Kang, Y. Han, and Y. Song. 2018. Spatial and temporal patterns of microclimates at an urban forest edge and their management implications. Environmental monitoring and assessment 190:93.

Lorenz, K., and R. Lal. 2005. The depth distribution of soil organic carbon in relation to land use and management and the potential of carbon sequestration in subsoil horizons. Advances in

agronomy 88:35-66.

Lorenz, K., and R. Lal. 2009. Biogeochemical C and N cycles in urban soils. Environment International 35:1-8.

Magnusson, S., K. Lundberg, B. Svedberg, and S. Knutsson. 2015. Sustainable management of excavated soil and rock in urban areas-a literature review. Journal of Cleaner Production 93:18-25.

Malmivaara-Lämsä, M., L. Hamberg, E. Haapamäki, J. Liski, D. J. Kotze, S. Lehvävirta, and H. Fritze. 2008. Edge effects and trampling in boreal urban forest fragments-impacts on the soil microbial community. Soil Biology and Biochemistry 40:1612-1621.

Mariotti, A. 1983. Atmospheric nitrogen is a reliable standard for natural ^{15}N abundance measurements. Nature 303:685-687.

Mazurek, R., J. Kowalska, M. Gąsiorek, and M. Setlak. 2016. Micromorphological and physico-chemical analyses of cultural layers in the urban soil of a medieval city—A case study from Krakow, Poland. Catena 141:73-84.

Miller, J. D., H. Kim, T. R. Kjeldsen, J. Packman, S. Grebby, and R. Dearden. 2014. Assessing the impact of urbanization on storm runoff in a peri-urban catchment using historical change in impervious cover. Journal of Hydrology 515:59-70.

Morra, M., M. Hall, and L. Freeborn. 1991. Carbon and nitrogen analysis of soil fractions using near-infrared reflectance spectroscopy. Soil Science Society of America Journal 55:288-291.

Norra, S., L. L. Handley, Z. Berner, and D. Stuben. 2005. ^{13}C and ^{15}N natural abundances of urban soils and herbaceous vegetation in Karlsruhe, Germany. European Journal of Soil Science 56:607-620.

Nowak, D. J., R. A. Rowntree, E. G. McPherson, S. M. Sisinni, E. R. Kerkmann, and J. C. Stevens. 1996. Measuring and analyzing urban tree cover. Landscape and Urban Planning 36:49-57.

Olsthoorn, A. F. M. 1991. Fine root density and root biomass of two Douglas-fir stands on sandy soils in the Netherlands. 1. Root biomass in early summer. Netherlands Journal of Agricultural Science 39:49-60.

Pavao-Zuckerman, M. A. 2008. The Nature of Urban Soils and Their Role in Ecological Restoration in Cities. Restoration Ecology 16:642-649.

Pouyat, R. V., I. D. Yesilonis, and D. J. Nowak. 2006. Carbon storage by urban soils in the United States. Journal of Environmental Quality 35:1566-1575.

Putz, S., J. Groeneveld, K. Henle, C. Knogge, A. C. Martensen, M. Metz, J. P. Metzger, M. C. Ribeiro, M. D. De Paula, and A. Huth. 2014. Long-term carbon loss in fragmented Neotropical forests. Nature communications 5:5037.

Raciti, S. M., L. R. Hutyra, and A. C. Finzi. 2012. Depleted soil carbon and nitrogen pools beneath impervious surfaces. Environmental Pollution 164:248-251.

Reinmann, A. B., and L. R. Hutyra. 2017. Edge effects enhance carbon uptake and its vulnerability to climate change in temperate broadleaf forests. Proceedings of the National Academy of Sciences 114:107-112.

Reinmann, A. B., I. A. Smith, J. R. Thompson, and L. R. Hutyra. 2020. Urbanization and fragmentation mediate temperate forest carbon cycle response to climate. Environmental Research Letters 15:114036.

Revelle, R., and H. E. Suess. 1957. Carbon dioxide exchange between atmosphere and ocean and the question of an increase of atmospheric CO2 during the past decades. Tellus 9:18-27.

Riutta, T., H. Clack, M. Crockatt, and E. M. Slade. 2016. Landscape-Scale Implications of the Edge Effect on Soil Fauna Activity in a Temperate Forest. Ecosystems 19:534-544.

Rogers, K. M., R. E. Turnbull, A. P. Martin, W. T. Baisden, and M. S. Rattenbury. 2017. Stable isotopes reveal human influences on southern New Zealand soils. Applied Geochemistry 82:15-24.

Rumpel, C., and I. Kogel-Knabner. 2011. Deep soil organic matter-a key but poorly understood component of terrestrial C cycle. Plant and Soil 338:143-158.

Ruwanza, S. 2019. The Edge Effect on Plant Diversity and Soil Properties in Abandoned Fields Targeted for Ecological Restoration. Sustainability 11:140.

Ryu, Y., T. Nilson, H. Kobayashi, O. Sonnentag, B. E. Law, and D. D. Baldocchi. 2010. On the correct estimation of effective leaf area index: Does it reveal information on clumping effects? Agricultural and Forest Meteorology 150:463–472.

Salgo, A., J. Nagy, J. Tarnóy, P. Marth, O. Pálmai, and G. Szabó–Kele. 1998. Characterisation of soils by the near infrared technique. Journal of Near Infrared Spectroscopy 6:199–203.

Salome, C., N. Nunan, V. Pouteau, T. Z. Lerch, and C. Chenu. 2010. Carbon dynamics in topsoil and in subsoil may be controlled by different regulatory mechanisms. Global Change Biology 16:416–426.

Scalenghe, R., and F. A. Marsan. 2009. The anthropogenic sealing of soils in urban areas. Landscape and Urban Planning 90:1–10.

Schleicher, N. J., Y. Yu, K. Cen, F. Chai, Y. Chen, S. Wang, and S. Norra. 2013. Source Identification and Seasonal Variations of Carbonaceous Aerosols in Beijing — A Stable Isotope Approach. Pages 263–270. Springer Netherlands, Dordrecht.

Singh, K. K., R. A. Bianchetti, G. Chen, and R. K. Meentemeyer. 2017. Assessing effect of dominant land–cover types and pattern on urban forest biomass estimated using LiDAR metrics. Urban Ecosystems 20:265–275.

Sizer, N. C., E. V. Tanner, and I. D. K. Ferraz. 2000. Edge effects on litterfall mass and nutrient concentrations in forest fragments in central Amazonia. Journal of Tropical Ecology 16:853–863.

Smith, I. A., L. R. Hutyra, A. B. Reinmann, J. R. Thompson, and D. W. Allen. 2019. Evidence for edge enhancements of soil respiration in temperate forests. Geophysical Research Letters 46:4278–4287.

Stevens, A., B. van Wesemael, H. Bartholomeus, D. Rosillon, B. Tychon, and E. Ben–Dor. 2008. Laboratory, field and airborne spectroscopy for monitoring organic carbon content in agricultural

soils. Geoderma 144:395-404.

Stevenson, B. A., R. Parfitt, L. A. Schipper, W. T. Baisden, and P. Mudge. 2010. Relationship between soil $\delta^{15}N$, C/N and N losses across land uses in New Zealand. Agriculture, ecosystems & environment 139:736-741.

Sung, W. G., D. K. Lee, and Y. Jin. 2018. Analyzing Difference of Urban Forest Edge Vegetation Condition by Land Cover Types Using Spatio-temporal Data Fusion Method. Journal of Environmental Impact Assessment 27:279-290.

Takahashi, T., Y. Amano, K. Kuchimura, and T. Kobayashi. 2008. Carbon content of soil in urban parks in Tokyo, Japan. Landscape and Ecological Engineering 4:139-142.

Thornton, B., G. Martin, M. Procee, D. R. Miller, M. Coull, H. Yao, S. J. Chapman, G. Hudson, and A. J. Midwood. 2015. Distributions of carbon and nitrogen isotopes in Scotland's topsoil: a national-scale study. European Journal of Soil Science 66:1002-1011.

Torn, M. S., S. E. Trumbore, O. A. Chadwick, P. M. Vitousek, and D. M. Hendricks. 1997. Mineral control of soil organic carbon storage and turnover. Nature 389:170.

Trlica, A., L. R. Hutyra, L. L. Morreale, I. A. Smith, and A. B. Reinmann. 2019. Current and future biomass carbon uptake in Boston's urban forest. Science of The Total Environment:136196.

USDA-NRCS. 1992. Soil Survey Laboratory Methods Manual. Soil Conservation Service U.S., Department of Agriculture, Rep. 42, Washington,. D. C.

USDA. 2010. Soil Survey Staff. USDA-Natural Resources Conservation Service, Washington, DC.

Vasenev, V. I., J. J. Stoorvogel, and Vasenev, II. 2013. Urban soil organic carbon and its spatial heterogeneity in comparison with natural and agricultural areas in the Moscow region. Catena 107:96-102.

Vasenev, V., and Y. Kuzyakov. 2018. Urban soils as hot spots of anthropogenic carbon accumulation: Review of stocks, mechanisms

and driving factors. Land Degradation & Development 29:1607–1622.

Viswanathan, B., A. Volder, W. T. Watson, and J. A. Aitkenhead–Peterson. 2011. Impervious and pervious pavements increase soil CO2 concentrations and reduce root production of American sweetgum (Liquidambar styraciflua). Urban Forestry & Urban Greening 10:133–139.

Wade, T. G., K. H. Riitters, J. D. Wickham, and K. B. Jones. 2003. Distribution and causes of global forest fragmentation. Conservation Ecology 7 (2): 7.

Wang, C., H. Wei, D. Liu, W. Luo, J. Hou, W. Cheng, X. Han, and E. Bai. 2017. Depth profiles of soil carbon isotopes along a semi–arid grassland transect in northern China. Plant and Soil 417:43–52.

Wei, Z. Q., S. H. Wu, X. Yan, and S. L. Zhou. 2014a. Density and Stability of Soil Organic Carbon beneath Impervious Surfaces in Urban Areas. PloS one 9:7.

Wei, Z. Q., S. H. Wu, S. L. Zhou, J. T. Li, and Q. G. Zhao. 2014b. Soil Organic Carbon Transformation and Related Properties in Urban Soil Under Impervious Surfaces. Pedosphere 24:56–64.

Wu, Q., H.–q. Li, R.–s. Wang, J. Paulussen, Y. He, M. Wang, B.–h. Wang, and Z. Wang. 2006. Monitoring and predicting land use change in Beijing using remote sensing and GIS. Landscape and Urban Planning 78:322–333.

Yan, Y., W. H. Kuang, C. Zhang, and C. B. Chen. 2015. Impacts of impervious surface expansion on soil organic carbon – a spatially explicit study. Scientific Reports 5:9.

Yost, J. L., and A. E. Hartemink. 2020. How deep is the soil studied – an analysis of four soil science journals. Plant and Soil.

Yuan, F., and M. E. Bauer. 2007. Comparison of impervious surface area and normalized difference vegetation index as indicators of surface urban heat island effects in Landsat imagery. Remote Sensing of environment 106:375–386.

Yun, H.–S., J.–Y. Lee, D.–Y. Yang, and S.–S. Hong. 2007. Areal Distribution Ratio of Rock ffes with Geologic Ages in the Gyeonggi–

Seoul-Incheon Areas. The Journal of the Petrological Society of Korea 16:208-216.

Zhang, X. F., X. Zhang, and G. H. Li. 2015. The effect of texture and irrigation on the soil moisture vertical-temporal variability in an urban artificial landscape: a case study of Olympic Forest Park in Beijing. Frontiers of Environmental Science & Engineering 9:269-278.

Zheng, D., J. Chen, J. M. LeMoine, and E. S. Euskirchen. 2005. Influences of land-use change and edges on soil respiration in a managed forest landscape, WI, USA. Forest Ecology and Management 215:169-182.

Chapter 5: Conclusion

1. Anthropogenic soil burial contributes urban deep SOC storage

In Chapter 2, our results showed that deep soils are hidden elements of the carbon budget in the urban region. We provided evidence that land use changes can lead to long-lasting effects on vertical heterogeneity of SOC stocks in urban areas. The magnitude of SOC stocks varied with land cover types and origins of SOC depended on the soil depths, which reflected the land use history. Our results highlight that deep soils under impervious surfaces could be overlooked carbon hotspots in urban ecosystems. More attention must be given to soils under impervious surfaces, which have been largely ignored in urban carbon budgets. We call more efforts to understand the deep SOC change mechanisms with urbanization across various spatial and temporal scales.

2. Heterogeneous human activities at urban forest edge lead to complex edge effects on SOC stocks

In Chapter 3, our results indicate that the magnitude and cause of edge effects on SOC stocks varied within fragmented landscapes, and that human activities alter SOC stocks in urban landscapes. The declines in above- and belowground biotic factors (i.e., LAI, NDVI, Lf and FRMD) observed in plots located closer to the rural forest edges underpin significant declines in SOC stocks. The differences of urban SOC stocks between the edges and interiors did not show clear patterns; however, the SOC stocks at the east edges (4.74 kgC m^{-2}) were 63% greater than at the west edges (2.9 kgC m^{-2}), and were explained by the adjacent land use and litterfall management practices. The impact of fragmentation on urban SOC stocks is due to more than just the direct effect of biotic factors; it also involves the indirect effects of human activities, which adds complexity compared to the impacts on SOC decline at rural edges. This latter effect is a key mechanism in the observed response to SOC change at urban forest edges. This study provides insight into the relationship between forest fragmentation and SOC stocks, which

involves a combination of natural and anthropogenic factors.

3. Soil spectroscopy has great potential to predict SOC in heterogeneous urban landscapes

In Chapter 4, our results indicated that the SOC can be estimated with reasonable accuracy across urban vegetated area based solely on the hyperspectral reflectance spectroscopy, and the strategy has the potential of upscaling for city scale assessments of SOC budgets. Specific objectives of this study include: 1) to quantify the spatial variations of SOC and $\delta^{13}C$ among different land cover; 2) to assess the potential for spectroscopy to predict for SOC and $\delta^{13}C$ under heterogeneous urban land cover types. The PLSR model achieved acceptable performance with coefficient of determination (R^2) and root mean square error (RMSE) of calibration set for SOC concentration (R^2 = 0.83; RMSE = 1.6%). The leave-one-out cross-validation (LOOCV) procedure confirmed the robust performance of PLSR model. According to the VIP scores, urban SOC in oven-dried soil samples can be accurately predicted by mean of visible (VIS, 400-700 nm) and near infrared (NIR, 2200-2300) diffuse reflectance spectroscopy (Fig. 4.4, 1>VIP). Despite these promising results, caution should be taken regarding the nature of sampling and number of samples analysed for developing prediction equations. Further work is needed to evaluate different soil depths with large sample size in order to expand the utilization of spectroscopy for SOC prediction in urban ecosystem.

Abstract in Korean

탄소 중립 도시를 위한 이질적 도시 피복 내 토양 유기 탄소 저장량 평가

배지환
서울대학교 환경대학원 협동과정조경학
논문지도교수: 류영렬

기후 변화 대응책으로 탄소중립 도시의 중요성이 증가하며, 도시 토양 탄소 평가 및 관리의 중요성 역시 강조되고 있다. 본 학위논문은 도시화 과정에서 수반되는 세 종류의 토양 환경 변화 요인: 1) 지하 개발, 2) 녹지 파편화, 3) 도시 팽창이 토양 탄소 분포에 어떤 영향을 미치는지 정량적으로 평가함과 동시에 효율적 도시 토양 관리를 위한 분광 기반 토양 탄소 예측 시스템의 잠재력을 평가하였다.

도시화에 따른 토지 피복 변화는 토양 탄소 저장 분포의 수평 및 수직적 교란을 동반한다. Chapter 2 에서는 도시 지하 개발이 야기하는 토양 탄소 저장 분포의 수직 교란을 불투수층 및 도시 녹지대에서 5 m 깊이까지 비교 평가하였다. Chapter 3 에서는 도시 개발로 파편화된 녹지 축을 선정하여, 토양 탄소 저장량의 가장자리 효과를 도시 녹지 및 도시 산림 부지에서 비교 분석하였다. Chapter 4 에서는 팽창하는 도시 속 효율적 토양 탄소 저장 평가 및 관리를 위해, 초분광 반사정보를 활용한 토양 탄소 예측 모델을 개발 및 평가하였다.

도시 토양 탄소 저장량 평가는 도시 녹지 표토의 탄소 저장능에 집중되어 왔으며, 도시를 대표하는 토지 피복 중 하나인 불투수층 아래 토양 탄소 평가는 기존 도시 연구의 한계점으로 인식되어왔다. 본 학위논문의 Chapter 2에서는 서울 강남의 아파트 단지들을 대상으로, 조경지 및 불투수층 아래의 토양 탄소 저장량을 5 m 깊이까지 평가하였다. 도시 토양 탄소 저장량을 5 m 깊이로 평가한 결과, 불투수층(16.9 ± 1.9 kgC m^{-2})과 조경지(22.3 ± 2.2 kgC m^{-2})에서 큰 차이를 확인할 수 없었다. 1 m 깊이 내 토양 탄소가 5 m 총 깊이에서 차지하는 비중 역시 조경지에서 34%, 불투수층 부지에서 16%인 것으로 평가되었다. 도시 심토층에 축적된 상당량의 토양 탄소

기원은 안정성 탄소-질소 동위원소($\delta^{13}C$, $\delta^{15}N$) 분석 결과, 과거 대상지의 주된 인간활동인 농경 활동의 영향으로 추정되었다. 즉, 아파트 개발 부지 내 과거 농경지 토양이 성토와 같은 인위적 교란으로 2-3 m 깊이에 장기간 저장되어 문화적층으로 오늘날 존재한 것이다. 이러한 결과는 기존 도시 토양 탄소 저장량이 과소평가된 가능성과 더불어 도시 개발 역사와 수직적 토양 교란이 도시 토양 탄소 저장능에 중요한 요소임을 시사한다. 한정된 토지 활용을 극대화하기 위한 지하 개발이 가속화되는 현대 도시에서 반출된 심토 내 높은 유기 탄소는 기후 변화 속 탄소 중립 정책을 위한 탄소 자원 및 조경 소재로 재사용될 수 있을 것이다.

도시화에 따른 녹지 파편화는 녹지 가장자리 면적을 급격히 증가시킨다. 녹지 가장자리와 중심부 사이 환경 조건의 차이는 생물적, 비생물적 가장자리 효과를 동반한다. 그러나, 토양 탄소 저장 분포의 가장자리 효과는 그 원인과 규모 측면에서 사례 연구가 부족하다. Chapter 3에서는 파편화된 도시 녹지 축을 대상지로, 토양 탄소 저장량의 가장자리 효과를 도시 숲과 산림지역에서 비교 분석하였다. 그 결과, 산림 가장자리로부터 20 m 거리내 토양 탄소 저장량(1.86 kgC m^{-2})은 산림 중심부(10.47 kgC m^{-2})와 비교하여 80% 낮은 것으로 평가되었다. 산림 가장자리의 낮은 토양 탄소 저장량은 토양 탄소 기원인 식생 미세 뿌리 함량(R^2 > 0.77), 연간 낙엽량(R^2 > 0.94), 엽면적 지수(R^2 > 0.92)와 같은 생물적 요소 감소로 설명되었다. 반면 도시 숲의 경우, 가장자리 인접 이질적 인간활동이 토양 탄소 저장량에 영향을 주는 것으로 분석되었다. 그 예로, 도시 숲의 동쪽(4.74 kgC m^{-2}) 및 서쪽(2.9 kgC m^{-2}) 가장자리 녹지는 가장자리 구조와 낙엽관리의 차이로, 비록 동일한 시기에 파편화되었더라도, 토양 탄소 저장량의 유의미한 차이를 보였다. 또한, 식생 생육 기간 내 표토의 온도(ΔT_S > 2.8℃)와 습도(ΔVWC > 0.05 m^3 m^{-3}) 역시 도시 녹지의 동쪽-서쪽 가장자리에서 유의미한 차이를 보였다. 이는 도시 가장자리 녹지는 생물적 요소 뿐 아니라 마주한 인접 토지 피복의 유형과 인간 활동이 토양 탄소 저장량의 이질적 가장자리 효과를 유도할 수 있음을 의미한다. 더불어, 낙엽 존치와 같은 토양 탄소원 관리를 통해, 낮게 평가된 가장자리 녹지내 토양 탄소 저장량이 향후 개선의 여지가 있음을 시사한다.

도시 토양의 유기 탄소는 다양한 인간활동과 이질적 도시 모질에서 기원한다. 도시 토양 관리 측면에서 유기 탄소 저장 및 기원 평가는

기후 변화 속 그 중요성이 강조되는 반면, 기존 화학적 분석법은 비용과 시간 측면에서 가속되는 도시 팽창에 대처하기 어렵다는 한계점을 갖는다. Chapter 4 에서는 분광계로 취득한 도시 토양 초분광 반사 정보(350−2,500 nm)를 활용하여, 도시 공원내 여섯 종류 토지 피복(혼효림, 침엽수림, 활엽수림, 잔디, 습지, 나지) 조건의 토양 유기 탄소 함량을 예측하는 분광기반 토양 탄소 예측 모델을 개발하였다. 또한, 이질적 도시 피복 내 토양 탄소 기원 추적을 위해, 안정성 탄소 동위원소($\delta^{13}C$) 역시 여섯 종류의 토지 피복 조건에서 평가하였다. 총 136개의 표토 샘플을 바탕으로 LOOCV 교차검증(leave−one−out cross−validation)을 실시하였으며, PLS(partial least squares) 회귀분석법을 통해 기존 화학적 분석법과 분광기반 평가법을 비교한 결과, 유기 탄소(R^2 = 0.83; RMSE = 1.6%) 추정에서 유의미한 예측 정확도를 확인하였다. 분광 기반 토양 유기 탄소 예측의 중요 파장대(1 > VIP; variable importance in projection)는 가시광선(400~700 nm) 및 근적외선(2200~2300 nm) 영역 일부가 주요함이 평가되었다. 이와 같은 결과는 분광 반사정보를 통한 도시 토양 탄소 예측이 높은 잠재력을 갖고 있음을 시사한다. 도시 공원내 여섯 토지 피복 중, 습지 토양 탄소 추정치가 화학적 분석법 대비 저평가 되었으며, 이는 습지 토양의 넓은 탄소 함량 범위 및 수생태계 기원 이질적 탄소원의 영향으로 추정된다. 이러한 한계점은 습지와 같은 특정 토지 피복의 개별 분광 라이브러리 구축 및 추정 모델 개발로 보완될 수 있을 것이다.

본 학위 논문에서 도출된 도시 토양 탄소 저장 특성의 공통 함의는 1) 과거 및 오늘날의 인간활동이 도시 토양 탄소 저장량 변화를 주도할 수 있으며, 2) 도시 생태계 특유의 수평 및 수직적 토양 탄소 분포 형태가 존재한다는 것이다. 이러한 도시 특유의 토양 탄소 분포는 3) 분광 기반 예측 시스템을 통해 도시 규모로 평가될 수 있으며, 이는 탄소중립 도시 정책 수립의 기초자료로 활용될 수 있을 것이다.

Keyword: 도시화, 토지 피복, 도시 토양, 도시 심토, 유기 탄소, 가장자리 효과, 안정성 탄소 동위원소, 토양 분광
학번: 2019−32756